University of Wisconsin Milwaukee
UWM Digital Commons

Theses and Dissertations

May 2013

Mechanics of Bolted Electrical Splices

Samuel Alberts
University of Wisconsin-Milwaukee

Follow this and additional works at: https://dc.uwm.edu/etd

 Part of the Mechanical Engineering Commons

Recommended Citation
Alberts, Samuel, "Mechanics of Bolted Electrical Splices" (2013). *Theses and Dissertations*. 92.
https://dc.uwm.edu/etd/92

This Thesis is brought to you for free and open access by UWM Digital Commons. It has been accepted for inclusion in Theses and Dissertations by an authorized administrator of UWM Digital Commons. For more information, please contact open-access@uwm.edu.

MECHANICS OF BOLTED ELECTRICAL SPLICES

by

Samuel Thomas Alberts

A Thesis Submitted in

Partial Fulfillment of the

Requirements for the Degree of

Master of Science

in Engineering

at

The University of Wisconsin-Milwaukee

May 2013

ABSTRACT

MECHANICS OF BOLTED ELECTRICAL SPLICES

by

Samuel Thomas Alberts

The University of Wisconsin-Milwaukee, 2013
Under the Supervision of Professor Ilya V. Avdeev

Localized heating of bolted electrical splices in the power distributing bus is a primary concern in the industrial automation industry. While localized heat generation problems are commonly reported in the field, it is not entirely clear what the root causes are. A methodology is presented for development of a tool to measure *in-situ* the influence of clamping load on the thermo-electric behavior of the splice joint. Applied research and reasoning used to identify probable root causes for failures reported in the field are also presented. Experiments were conducted to characterize the mechanical properties of the bolt and nut system used in service. A bolt was modified and retrofitted with strain gauges. This system was calibrated as a load cell and experiments were conducted to develop a sample specific model for determining the bolt pretension as a function of torque applied to the nut. The methods herein described can be implemented for applications in which optimal performance of bolted connections is required. Measurements were made of the electrical contact resistance and an idealized finite elements simulation of the contacting bus materials was studied alongside real samples. Based on this study, the author presents potential root causes for the onset of problematic localized heat generation.

TABLE OF CONTENTS

LIST OF FIGURES

LIST OF TABLES

ACKNOWLEDGEMENTS

First, and foremost, I would like to thank my older brother, Elias Alberts, who inadvertently taught me that if I couldn't find the tool to do the job, I should make my own tool. I would like to thank my advisor, Dr. Ilya Avdeev, for support and guidance. I would also like to thank my thesis committee, Dr. Ben Church and Dr. Michael Nosonovsky, for contributing their time and their expertise. I would also like to thank Dr. Anoop Dhingra for selecting me as the Lead Teaching Assistant for ME-111: Engineering Fundamentals for the past three semesters.

I would also like to thank my manager, Paul Krause, with the Low Voltage Motor Control Centers product development group at Rockwell Automation for essentially seeding the project and for providing an excellent working environment for the past two years. Also to my colleague, Troy Bellows, for teaching me how to be an engineer. I should also thank Juli Pickering, of CEAS Career Services, for helping me to land that first job and for always being available to provide career advice.

I would like to thank Subhashini Gunashekar for getting me acquainted with the tensile testing machine and Mark Palbicki for the time he spent helping me learn how to properly use the manual mill and lathe while I was an undergraduate.

I would like to thank my close friend and mentor, Dr. Robert T. Balmer, for urging me to pursue graduate studies, my parents, Melissa Laney and Dr. Thomas Alberts, for a lifetime of support, and my friends and fellow engineers and UWM Master's degree graduates, Austen Scudder, Mir Shams, and Paul Sisneros for being sounding boards for ideas, for inspiration, and for advice.

CHAPTER 1. Introduction

1.1 Motivation and Objectives

Industrial automation is the blanket term for the use of computer technology and feedback control logic in industry. In general, the implementation of control logic involves feeding particular inputs into a system, called the plant, to get a desired output [1]. In the industrial automation industry, the plant can range from an entire facility, manufacturing process or a particular apparatus. Examples include computer numerical control of machining processes, pressure or displacement controlled stamping and forming processes, and temperature control of various thermally sensitive processes. In practice, the industrial automation system is a power distribution network that feeds power from the facility main to lumped groups of individual power loads. Current, typically ranging from 800 Amps to 3000 Amps, nominally, is conducted via a conductive bus that is often a rigid and uninsulated. The bus is not insulated because it is housed inside of metal power containment structures which are subject to rigorous regulation imposed by various external agencies, such as Underwriters Laboratories, National Electric Manufacturers Association, and International Electrical Commission.

Overheating is a prevalent problem in industrial automation. Heat generation in the power control structure is a function of many parameters. By virtue of the application, heat is generated in response to high currents conducted by the bus. Heating problems most often occur at locations where one portion of main bus is spliced with another or where secondary, load, bus is spliced to the main bus. Sections of the bus structure are typically spliced together with bolted connections. Bolted splice connections are chosen because this allows for modularization of the rigid bus system components. The fact that

bolted splice joints can be assembled with inexpensive steel bolts, thus eliminating the need for expensive welding processes, is another economical impetus to use them. On the other hand, the quality of electrical conduction through the joint is a function of the quality of surface to surface contact between the sections of bus. There is potential for relatively high local heat generation to occur at the splices because conductivity is greatly reduced at the splice.

A common practice for locating and mitigating heat problems in the field is to open up the structure containing the bus system, image each splice with an infrared camera, and evaluate whether or not the temperature is acceptable. This methodology is time consuming, expensive, and can pose great safety risk as the bus is exposed and subject to an arc flash event. The author is pursuing a novel methodology for modeling and monitoring the temperature of the bus without opening the containment structure. Various specifics of this methodology are proprietary, as such; the author is not at liberty to describe all of them in this text. Instead, this text will is focused on development of an *in-situ* measurement tool, and method for characterizing the mechanical parameters of the bolted splice joint as well as identification of potential root causes to localized heat generation in the field.

The heat generation in the splice joint is primarily a function of material properties of the conductive surfaces in contact, clamping pressure between surfaces in contact due to bolt system pretension, and the surface quality of materials in contact. These three primary parameters are process and sample specific and cannot be explicitly solved for without use of empirical relations. In order to properly understand the heat generation

properties of a specific bolted splice joint system, engineers must gather real data from product samples which are manufactured according to organization specific tolerances.

Experiments were conducted to characterize the mechanical properties of the bolt and nut system used in service. A bolt was modified and retrofitted with strain gauges. The bolt with strain gauges was calibrated as a load cell and experiments were conducted to develop a sample specific model for determining the bolt pretension as a function of torque applied to the nut for *in-situ* studies. The calibration of the load cell was validated using an industry clamping pressure load cell. Bolts and nuts used in service were used to splice samples of bus material and the electrical resistance was measured across the interface in order to get an understanding of the relationship between applied clamping load and resistance. Bolt system pretension values computed with the experimental model were applied with finite elements analysis to produce a qualitative understanding of ideal contact between the conductors. The simulated contact pressure map was visually compared with real assembled samples of bus material. Finally, bolts and nuts used in service were used to splice samples of bus material and the electrical resistance was measured across the interface in order to get an understanding of the relationship between applied clamping load and resistance.

The methodology behind a proper test process should be repeatable and reliable. It should also be transferrable between testing operators. The author has placed particular emphasis on presenting the procedures and methods used throughout the project as transparently as possible such that they can be repeated with this text, alone, as a guide.

1.2 Literature Review

1.2.1 Theoretical Approach to Predicting Pretension in Bolts

In a technical article submitted to Mechanical Engineering magazine, J. H. Bickford cited as many as 76 different variables of interest for determining the pretension in a bolt [2]. Unfortunately, the industry standard is to assemble bolted joints with specified torque values which are essentially accepted based on experiential reasoning without consideration of the age of the bolt or lot-to-lot bolt variation. Depending on the application, this may be acceptable, but should not be preferred where high performance is expected.

The diagram in Figure 1-1 below describes the geometry of threaded fasteners. The terminology in the diagram will be used throughout this text.

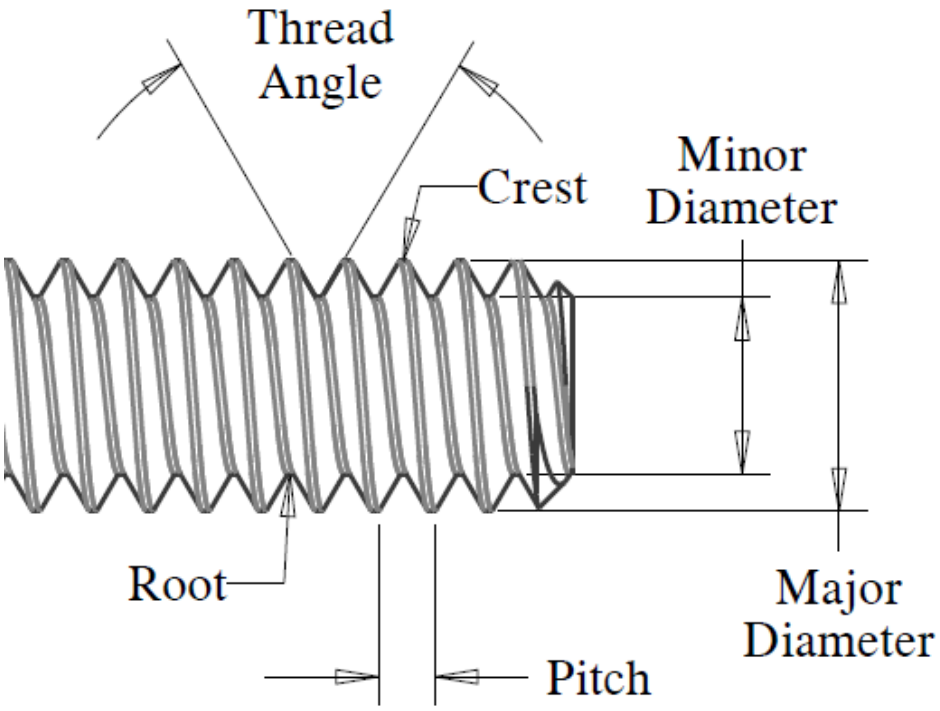

Figure 1-1. Diagram of Fastener Thread Geometry.

The primary geometric parameters that influence the mechanical behavior of the threaded fastener are thread angle, pitch, minor diameter, and major diameter. These parameters have been standardized for various sizes of threaded fastener by the Unified Thread Standard This standardization provides an increase in the predictability of behavior of bolted joints by reducing the gross randomness in thread geometry to a tightly defined tolerance window.

In practice, the tensioning of a bolted joint system is provided through applied torque on the nut. This can be described by adapting Shigley's description of the power screw by "unrolling" one revolution of screw thread as shown in the diagram in Figure 1-2 [3].

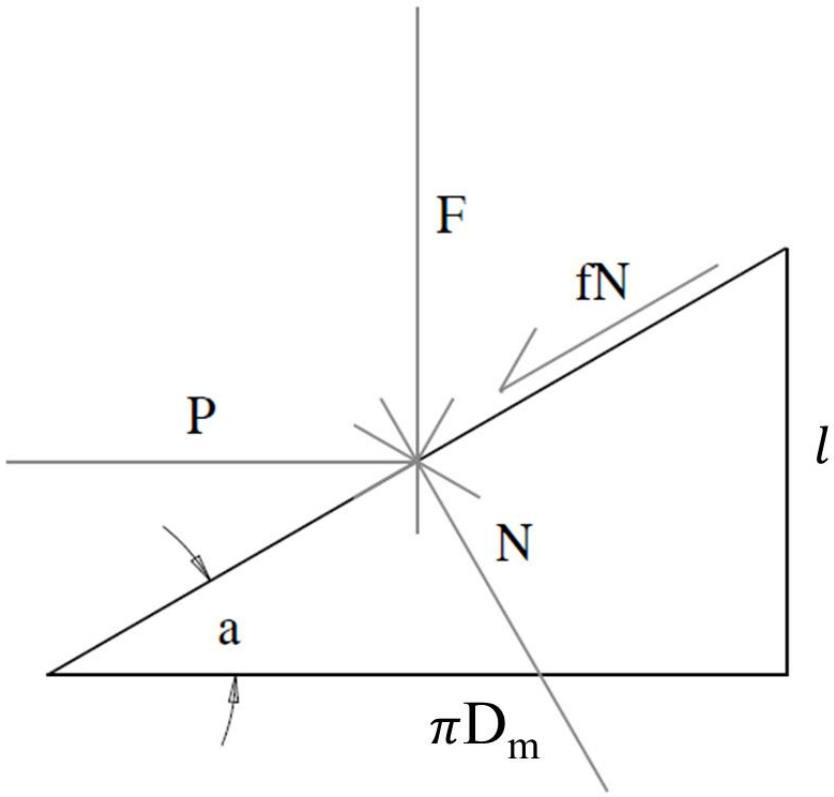

Figure 1-2. Diagram of Forces Acting on the Screw Thread.

In this diagram, D_m is the mean of the major and minor diameter, πD_m is then the mean circumference of the bolt, and the tangential distance a point at the mean diameter of the bolt will travel over one revolution. The variable, l, is the axial distance the point on the mean diameter of the bolt will progress as the bolt is rotated, which is commonly called the pitch. Regarding forces, P is a tangential force as a result of applying torque to the bolt which causes the thread to progress with respect to the mating thread, N is the normal reaction between thread surfaces, and fN is the friction force existing between the two surfaces. The remaining force, F, is the force acting axially to the shaft of the bolt and can be described as causing pretension in the bolt. As the bolt thread progresses

through the nut and constrains the clamped bodies, the bolt thread can no longer progress freely as torque is applied and the axial reaction, F, or pretension increases.

In a bolt splice, the bolt acts as a heavy spring to clamp the two conductor materials together. Pretension is required in the joint because if the system is left with zero pretension in the bolt changes in the system will dissolve the clamping action, resulting in opening of the clamped joint [4]. In general, there is typically a 2% to 11% drop in bolt pretension immediately after torqueing [5]. This is likely due to the influence of friction on the system as torque is applied. As torque is applied only about 10% of the applied torque contributes to clamping tension, the remainder of applied torque is necessary to overcome friction between the thread surfaces and between the clamped surface and the nut [6]. This initial relaxation is primarily elastic and is likely due to the release of the torque load on the system. There is also a time dependent relaxation which occurs. One study of A325 and A354 steel bolts showed an additional 4% relaxation over the course of 21 days [7]. Relaxation is of even more concern for the bolts in a bolted splice joint of conductors under current load as the materials used in bolts (typically steel for the application of interest) are temperature sensitive and subject to thermal relaxation over time [8]. Moreover, the thermal expansion of the conductor material (typically copper, which has a linear thermal expansion coefficient roughly 120% higher than steels [9]) will increase the transient relaxation of the bolt, which is commonly expected to be in service for years at a time. This can lead to a recursive behavior in which increasing heat generation and reduced contact pressure contribute to each other.

Since the geometry is standardized for all fasteners used in industry, friction is the primary governing agent of concern when designing for the development of bolt

pretension. Unfortunately, the friction behavior is highly process specific and cannot necessarily generalized for. For example, in some cases, design intent drives engineers to use titanium because of its good strength-to-weight ratio. In general, one would expect the amount of pretension derived from applied torque to vary across different material interfaces due to the variation of coefficient of friction. Croccolo et al. found that the use of titanium bolts threaded into steel base material leads to a situation where bolt pretension and clamping load development as a function of friction is found to vary based the choice of lubricant and number of times the system was disassembled and reassembled [10]. In a study on aluminum bolted joints, Croccolo et al. found that for a particular sample set, the pretension could vary by more than 300% based on surface preparation and that the friction behavior of coated thread surfaces would change with each loosening and tightening operation due to the removal of the coating [11]. A study by Eccles et al. showed a similar behavior in zinc plated fasterners [12]. One study showed that a bolt used in an airplane wing which had been disassembled and reassembled failed because the frictional behavior had changed between the time of initial assembly and the time of reassembly, years later [13].

1.2.2 Theory of Micro-Scale Contact Resistance

An electrical contact has been defined by Ragnar Holm as "a releasable junction between two conductors which is apt to carry electric current [14]." This is commonly seen in consumer products in the form of switches, such as those for turning on and off devices, and connectors, such as a USB connector for streaming data between devices. In the industrial automation industry, and power distribution in general, conducting releasable junctions are used in service for various purposes. Some examples are clamped

bus-bus splices, sliding bus-stab connections between individual loads and the power distribution bus, and industrial switchgear for opening and closing circuits for safety and maintenance purposes.

All real surfaces, no matter how well prepared, are “rough” at the microscopic level. That is, all real surfaces feature what are called “surface asperities.” These are microscopic peaks and valleys on the surface which result from manufacturing processes and material structural properties. Braunovic, et al. provide an in-depth discussion on the science of surface quality as well as methods for measuring the surface parameters [15]. The theory of electrical contact resistance is well understood on the basis of conduction constriction through single points of surface contact as a result of microscopic surface roughness [16]. As two conducting surfaces come into contact, the individual microscopic peaks mechanically contact each other. Force applied to clamp the surfaces together causes the peaks to break through the oxide film on the material surface and a cold weld occurs, allowing electrical conduction through the interface. Such a point is called an “a-spot” in electrical contact theory. Electrical conduction through the a-spot forces the theoretical lines of current to “constrict” and it becomes more difficult for electrons to flow through the constriction than it is for them to flow through the bulk of either contacting material. This is a function of the mean free path for flow of electrons in the material. The concept is shown in Figure 1-3 below. Timsit describes this phenomenon in explicit detail in his chapter of the book Electrical Contacts.

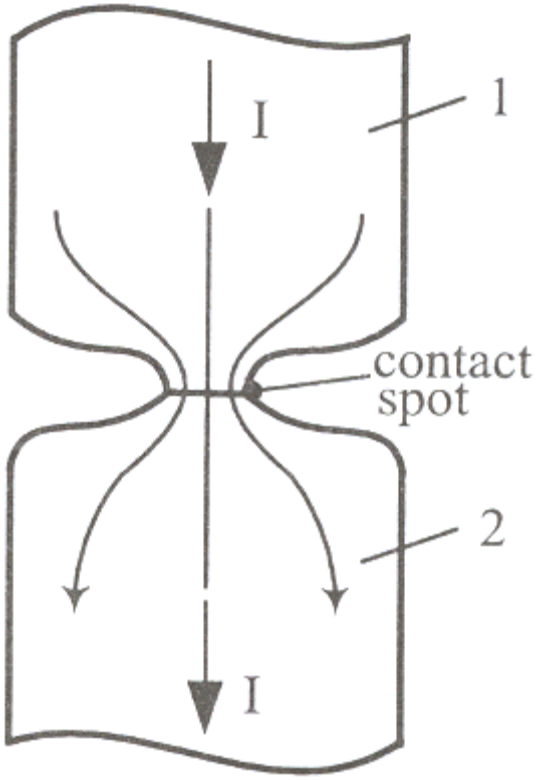

Figure 1-3. Graphical Description of Current Constriction Resistance.

As the applied clamping force is increased, the constriction resistance through the joint is expected to drop. This is a function of the increasing number of surface asperities in contact, as well as elastic and plastic deformation. To exemplify this, consider the interface of conductive surfaces as resistances in parallel. It is commonly understood from circuit theory that the reciprocal of the total resistance across a bank of resistors in parallel is equal to the sum of the reciprocals of each resistance in the bank. This is described by the following equation,

$$\frac{1}{R_T} = \sum_{i=1}^{n} \frac{1}{R_i} \ ,$$

in this equation, R_T is the total resistance across n resistances and R_i is an individual resistance. As the clamping load increases, the initial points of contact will deform, allowing additional surface asperities to come into contact, thus reducing the overall resistance of the interface. Contact interface resistance is a primary concern in the development of reliable micro-electromechanical systems (MEMS) because the scale of surface roughness is similar to the overall scale of the device [17 - 19]. A macro-scale process of interest for which the electrical contact resistance as a function of the surface quality is of key importance is resistance welding [20]. Research efforts to characterize the quality of surface contact regarding the size and spatial distributions of contact points include the development of deterministic asperity models [21], statistical and random process models [22, 23], and fractal geometry models [24]. Barber developed a boundary value approach to the contact resistance problem by considering geometric properties of the contacting areas studied the influence of statistical surface characteristics [25].

Approaching the design of electrically conductive surfaces for optimally reduced contact resistance from a micro-scale perspective is an applicable methodology in MEMS technologies. However, in the problem of interest, the variation of mating surfaces from nominal flatness due to geometrical tolerance allowances requires that the micro-scale approach to the design of the electric splice be foregone until these macroscopic issues are be dealt with. On the other hand, when addressing the mitigation of failure of the electrical splice, defined hereon as elevated heat generation in the region of the electrical contact, the engineer must be aware of and understand the micro-scale physics which govern the electro-thermal behavior of splice.

1.2.3 Bus Material and Degradation of Conducting Surfaces

The bulk of the studied bus material studied is a copper alloy, C11000. It is specified by ASTM as a bus bar, due to its rectangular profile [26]. Aluminum is also an option for bus material, but is less frequently used. Discussion in this text will stay focused on copper as a bus material. The copper bus material is tempered to a minimum hardness of Rockwell F 80. The material is either cold-drawn or rolled and then sheared to length by the manufacturer. The bus is electroplated with a layer of tin. Silver plating is also used for some applications. The discussion will stay focused on tin plating because it is more common in the field. Plating is introduced in order to reduce the formation of surface oxides [27]. Tin is noted as a particularly easy metal to electroplate in a controllable manner and thus provides an economical option for protection of the bus [28]. While tin is more resistive than copper, the detrimental influence of this increased resistance is decreased by requiring that the plating be very thin. In this particular case, the plating is specified to be on the order of 0.0002 inches thick. Tin is also less hard than copper and may provide for a more consistent surface to surface contact through plastic deformation of the a-spots. On the other hand, tin has a low melting point and is easily solderable. This amplifies the concern for temperature control of the bus and may lead to localized welding of bus-stab joints in the case of current overloads at junctions between individual loads and the bus.

Common mechanisms for degradation of the quality of the conductive interface are oxidation, fretting, stress relaxation, and thermal expansion. The topics of thermal expansion and stress relaxation were mentioned in Section 1.2.1. These two mechanisms recursively affect one another as the bus material expands at a higher volumetric rate than

the steel bolts in the splice joint, which leads to increased pretension in the bolt. Transient stress relaxation of the bolts occurs due to exposure to elevated temperature, as described with experiments on steel wires [29]. This, in turn, reduces the clamping load on the interfacing conductive surfaces, increasing the resistance across the interface. Oxidation is can be particularly damaging to the conductivity of the interface because metal oxides have a much higher resistivity than the pure metal. In the case of copper, the oxide is 10^{10} times more resistive [30]. Copper will oxidize immediately upon exposure to oxygen in the surrounding ambient atmosphere. As mentioned previously, this justifies the plating of the bus material with tin, which oxidizes much slower. On the other hand, the rate of oxidation of the bus is commonly a function of fretting wear, which cannot necessarily be controlled by design. Fretting wear is mechanical damage caused by low-cycle small amplitude relative motion between surfaces in contact [31]. In the industrial control power bus, fretting corrosion is likely caused due to ambient environment vibration, vibration resulting from processes occurring in the facility, or cycling of thermal expansion and contraction due to the power network being taken offline periodically for maintenance. Fretting causes new oxides to form as virgin material is uncovered by the fretting action which scrapes off the most outer material. In the worst case, over years of service, the base copper material may be exposed. This would result in a drastic increase in electrical contact resistance and thus, the likelihood of failure of the splice. Bryant and Antler provide very detailed descriptions of the effect on electrical contacts, in general, in their respective papers [32, 33].

CHAPTER 2: Correlation of Bolted Joint Torque and Pretension

The first immediately controllable factor governing the electro-thermal behavior of the splice joint is the pretension in the bolts which clamp the splice joint. As this is a function of bolt and nut materials, processing, and geometry a thorough understanding of the mechanical behavior of the bolt and nut in the bolt splice system is required to implement proper thermal modeling and monitoring of the industrial power distribution network. In Section 2.1, a rigorous approach to characterizing the material of the bolt and nut in service is presented. In Section 2.2, a bolt is modified and retrofitted with strain gauges in a half bridge configuration and calibrated as a load cell to measure the pretension in the bolt as a function of applied torque. Section 2.3 describes experimentation to correlate bolt pretension to applied torque and provides a benchmark against a theoretical calculation as well as bolt pretension data measured with a market clamping force load cell.

2.1 Bolt and Nut Test Sample Material Characterization

2.1.1 Experimental Samples and Apparatus

All bolt samples used throughout this study are round head square neck carriage bolts with geometry according to American Standard B18.5 [34]. They are cold headed medium carbon steel which is cold rolled threaded to 3/8”-16 UNC 2A according to American Standard B1.1 [35]. After forming, the bolts are tempered and quenched to Grade 5 quality hardness. This type of bolt is typical to those which may be used in bolted splice joints in industrial power distribution networks. According to internal

drawing tolerances, these bolts are expected to have nominal ultimate tensile and yield stresses of 120,000 and 92,000 pound-force per square inch, respectively.

Nine bolt samples were modified such that they matched the geometry of the bolts used as load cells as described in the next section. The bolts had a 0.33 inch long section of material removed 0.15 inches from the underside of the bolt head on a manual lathe. The threads were cut away to the minor diameter of the bolt shaft. The nominal minor cross sectional area according to the above threading geometry standard for these bolts is 0.068 square inches. The geometry is shown in Figure 2-1. The measured diameter in the machined section of each sample is presented below in Table 2-1. Based on a typical industry standard of plus-or-minus 0.005 inches tolerance on dimensions defined to the thousandths place, it would seem that the majority of samples were not within specification. This is likely a due to manual preparation of test samples.

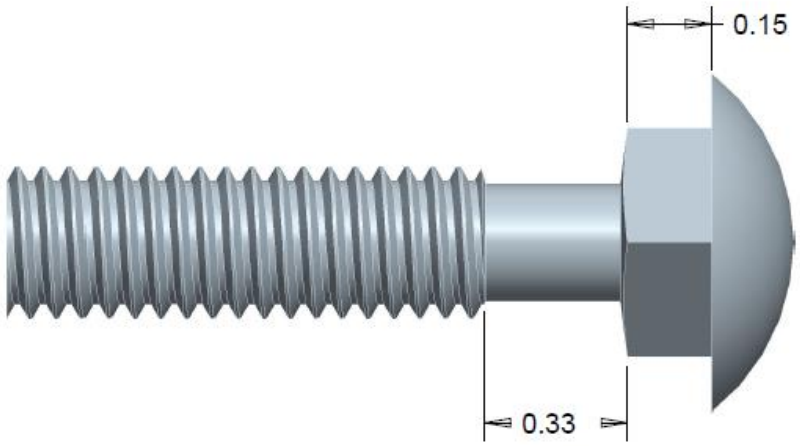

Figure 2-1. Carriage Bolt CAD Model and Modification Dimensions.

Nine additional bolts were selected for testing but were not modified. It was chosen to test the unmodified bolts in order to highlight any effects on material behavior resulting from modification of the bolts.

Tensile loads were applied to the bolt samples using a SATEC tensile testing machine. For the materials characterization process, the samples were tested at a constant pull rate of 0.2 inches per minute. Custom tensile grips were manufactured to apply the tensile load. The grips were reverse engineered from an existing set to provide the function of constraining a 3/8-16 bolt. One grip has a hole, tapped with 3/8”-16 threads while the other has a hollow core to allow for the bolt head and a hole on the bottom to pass the bolt shaft. A representative picture of the grips is shown in Figure 2-2 while dimensional drawings of the grips are presented in Appendix A.

Table 2-1. Geometry of Modified Bolt Samples

Sample	Test Section Area (in^2)
1	0.056
2	0.057
3	0.063
4	0.063
5	0.054
6	0.059
7	0.059
8	0.060
9	0.063

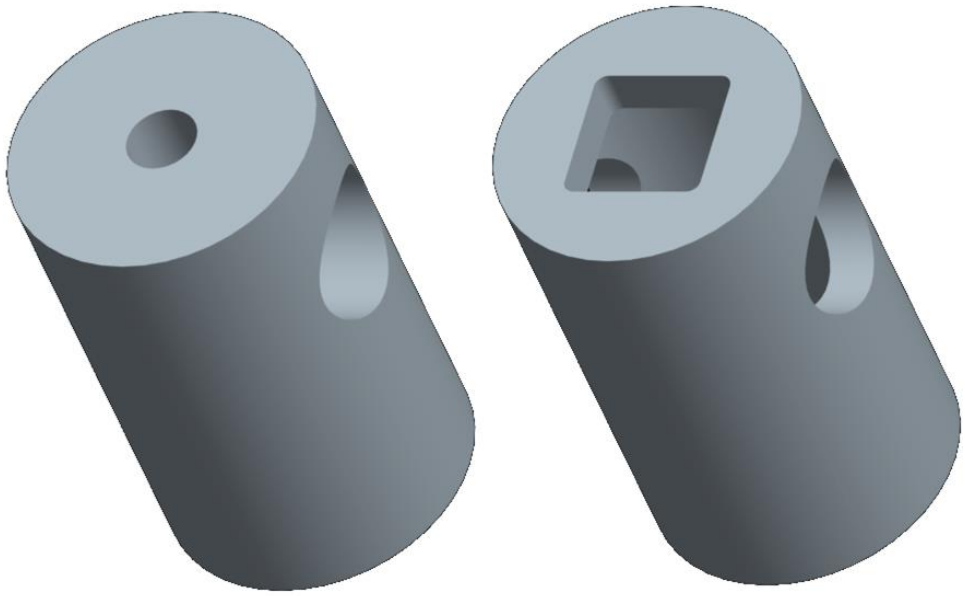

Figure 2-2. Tensile Grips Manufactured for Materials Characterization and Calibration Processes. (Left) Threaded Grip. (Right) Bolt Shaft Pass Grip.

All nut samples used in this experimentation are 3/8”-16 steel nuts with integral conical washers. This nut is representative of what may typically be used in bolted splice joints in industrial power distribution networks. The nut is connected to the washer by a flange which is swaged around a lip on the inner diameter of the washer. The nut and washer may rotate freely with respect to each other. The nut and washer configuration is shown in the section view in Figure 2-3.

Figure 2-3. Macro Photograph of Sectioned Nut and Integral Washer.

As torque is applied to the bolt system, leading to increased pretension in the bolt, the conical washer flattens elastically under the compressive load applied by the nut. Due to the developed stress profile in the washer in the flattened state, it will push back against the nut, providing a greater amount of friction between the nut and the clamped object [36]. This increases the stability of the clamping in the bolted splice joint and may play a role in the development of pretension in the bolt.

To provide insight to the influence of the flattening of the conical washer on the development of pretension in the bolted splice joint of study, 7 samples were tested in compression using the SATEC tensile testing machine. Compression was applied using a constant displacement rate of 0.2 inches per minute.

2.1.2 Materials Characterization Data

Since the tensile grip which holds the bolt head is a bearing contact, there was considerable variation from sample to sample in the amount of system settling which occurred before the stress profile began to develop. Each set of sample data was manually pre-processed to eliminate this portion of the data. The data were then processed and plotted using a MATLAB script and are presented in the following Figures. The MATLAB script was developed to streamline future work which is will likely involve many more tested samples in order to develop a better statistical representation of the material behavior. The script is presented in Appendix B. Stress-strain and stress-strain slope curves of all machined samples are presented in Figures 2-4 and 2-5, respectively. Stress-Strain and stress-strain slope of unmodified samples are presented in Figures 2-6 and 2-7, respectively. All samples from both sets are presented in a composite plot to allow for simplified comparison between individual samples. The slope of stress-strain plots were generated by computing the slope between consecutive points and then plotting this against the percent of average yield strength for the grouping of samples. In Figure 2-8 the average stress-strain curve for machined bolts is plotted along with the average curve for unmodified bolts to provide for comparison of the shapes of the corresponding stress profiles. For this same purpose, the average slope of stress-strain curve for machined bolts is plotted along with the average slope of stress-strain curve for unmodified bolts in Figure 2-9. Table 2-2 shows the average yield and ultimate tensile stresses for both machined and unmodified samples.

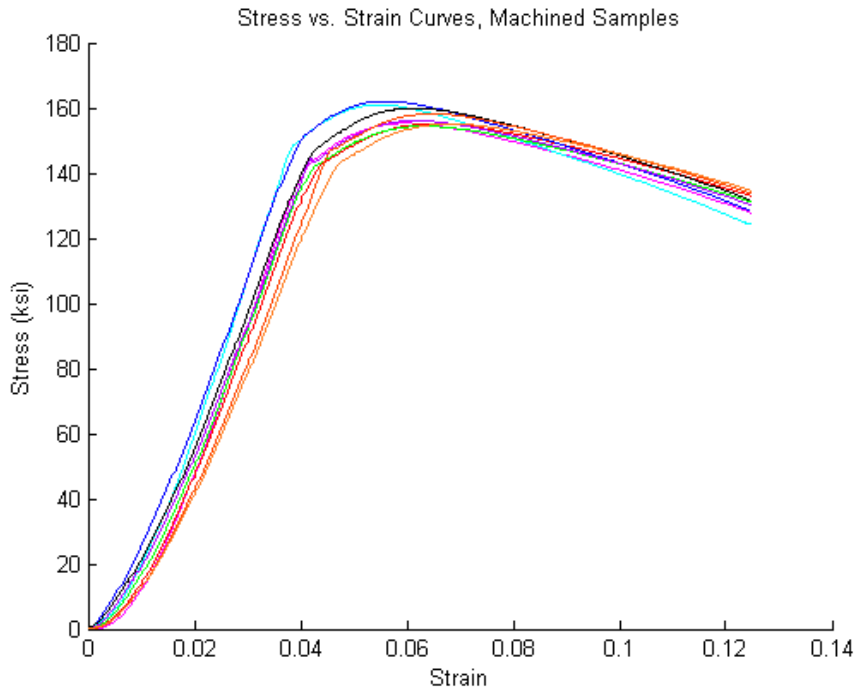

Figure 2-4. Composite Stress-Strain Curves for 9 Machined Samples

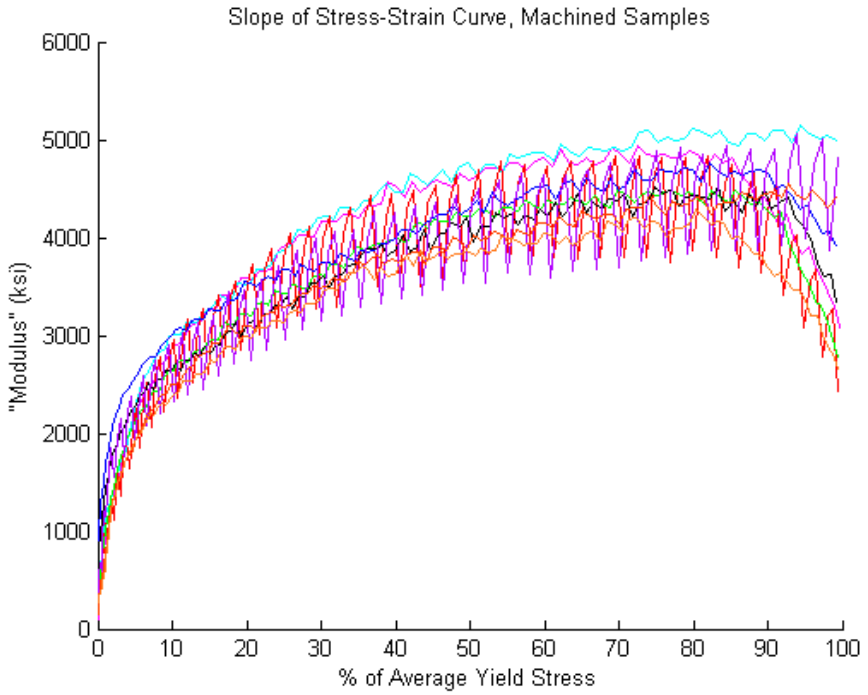

Figure 2-5. Slope of Stress-Strain Curves for 9 Machined Samples.

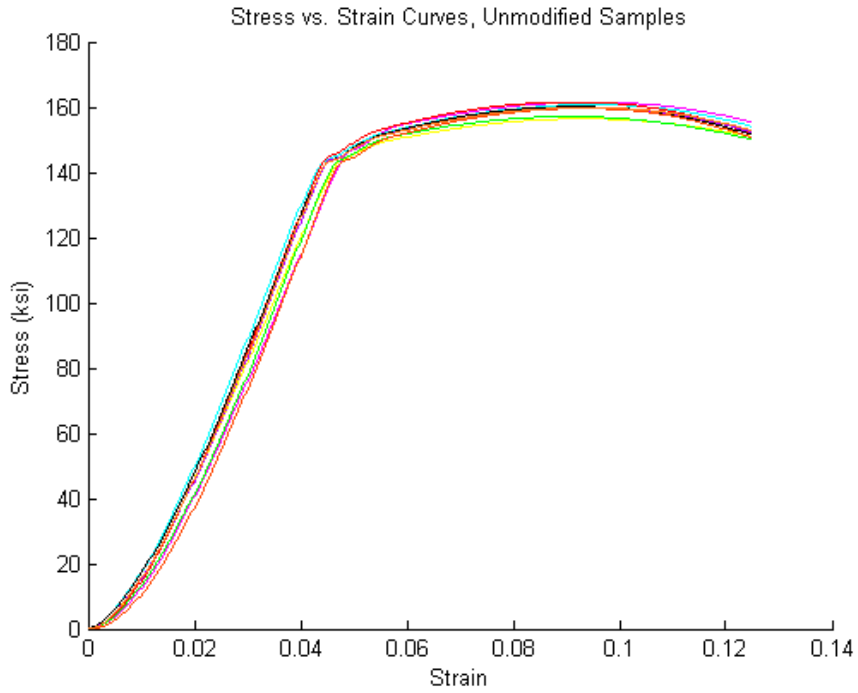

Figure 2-6. Composite Stress-Strain Curves for 9 Unmodified Samples.

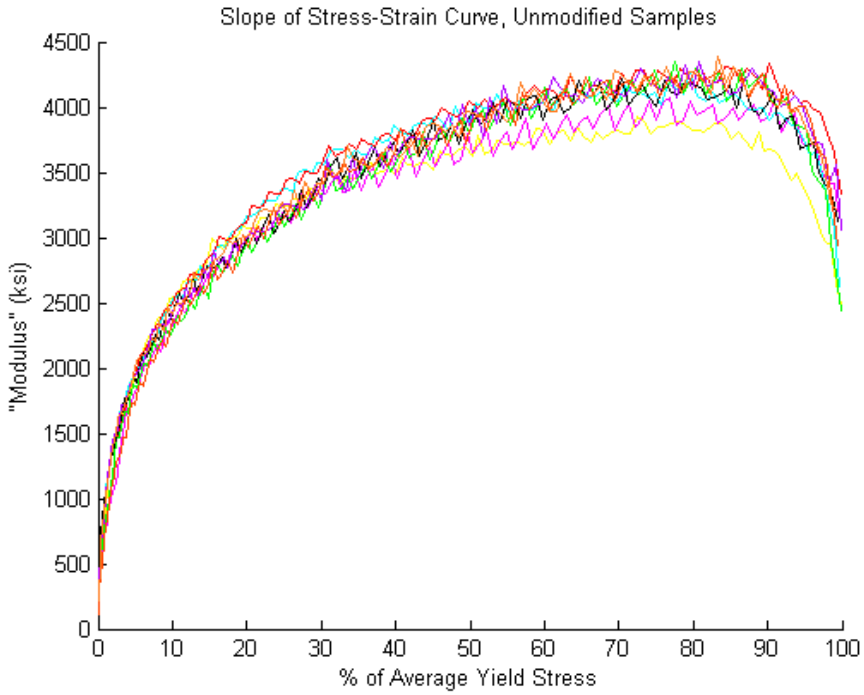

Figure 2-7. Slope of Stress-Strain Curves for 9 Unmodified Samples.

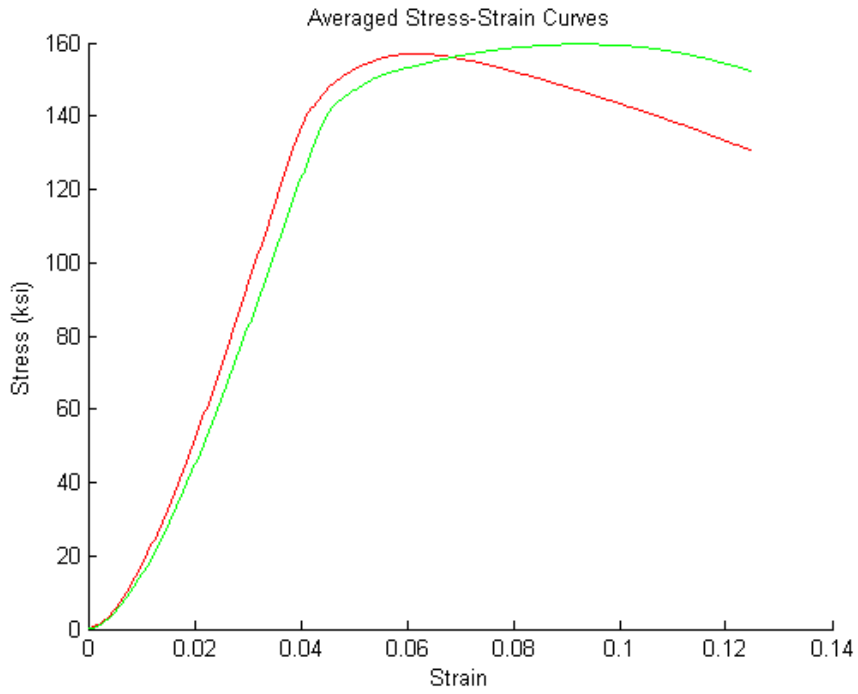

Figure 2-8. Averaged Stress-Strain Curves.
Machined (Red) and Unmodified (Green) Samples.

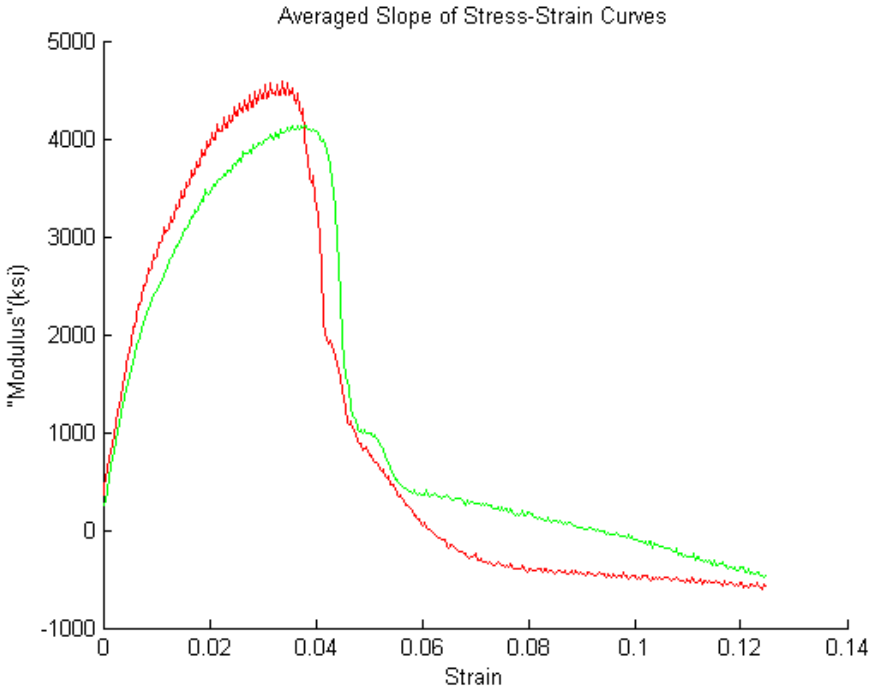

Figure 2-9. Averaged Slope of Stress-Strain Curves.
Machined (Red) and Unmodified (Green) Samples.

Table 2-2. Average Experimental Yield and Ultimate Strengths.

	Strength (psi)	
	Yield	**Ultimate Failure**
Machined	140,000	157,000
Unmodified	141,000	160,000

The nut compression data were also manually processed to isolate the data of interest. The data were processed using the MATLAB script listed in Appendix C. A composite plot of compression load against deformation for all samples along with the data average is presented in Figure 2-10. Figure 2-11 shows the slope of the load-deformation lines plotted against compressive load for all samples along with the data average. In both plots, the average is shown as a bold dashed black line while individual samples are thin colored lines.

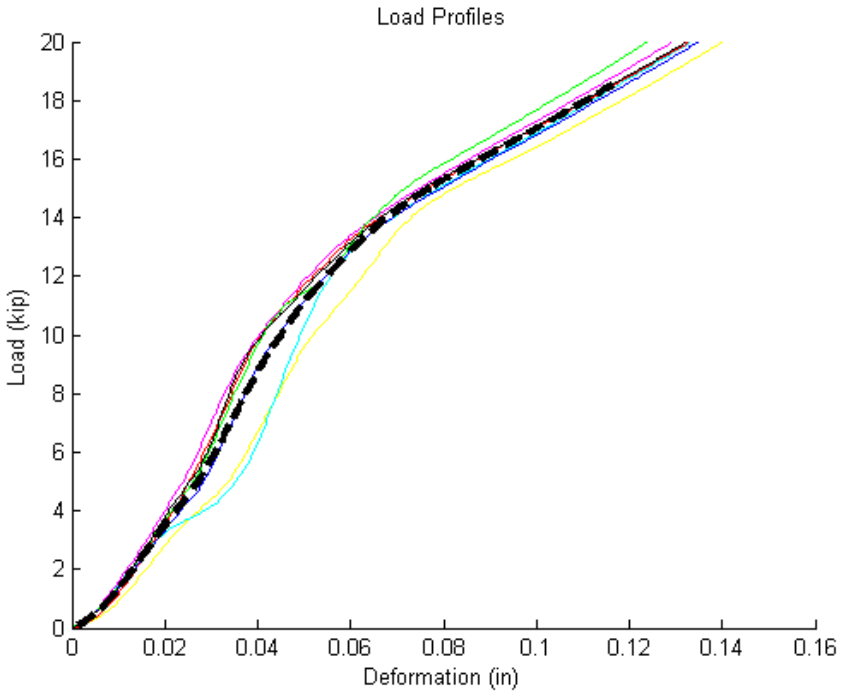

Figure 2-10. Individual Sample and Average Compression Load for Nut Samples.

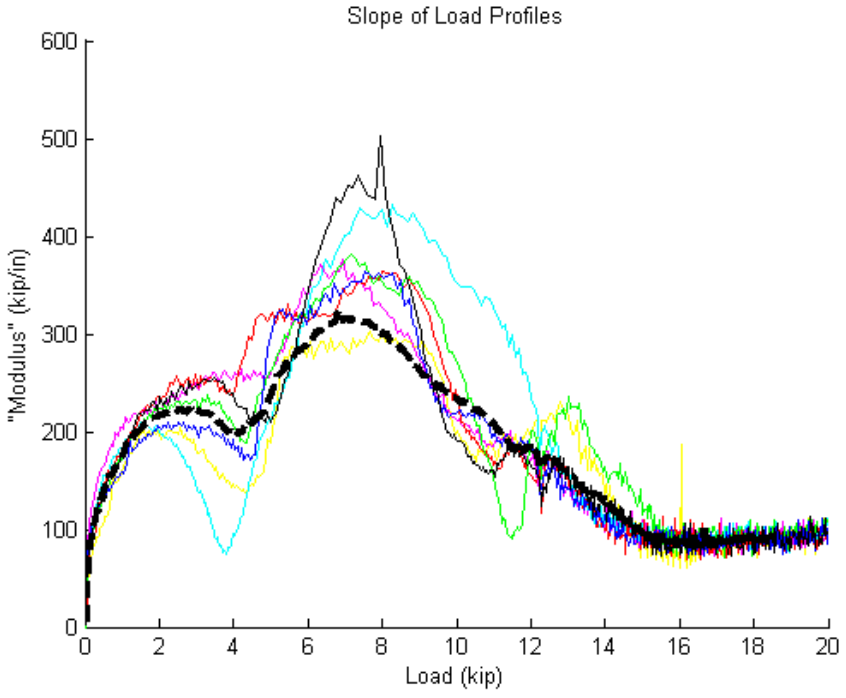

Figure 2-11. Individual Sample and Average Load-Deformation Slope for Nut Samples.

2.1.3 Discussion

In general, for both the machined and unmodified test samples, the material outperforms the nominal expectation. Both machined and unmodified samples exhibited yielding and ultimate failure at similar values of stress. Both sets of samples show considerable spread in the data. Overall, the spread in stress-strain data for both machined and unmodified samples can primarily be attributed to variations in the materials at the grain structure level, as well as design tolerances for the rolled threading and heat treatment processes. Also, since the head of the bolt is cold formed there is some tolerance allowance in the concentricity of the bolt shaft with respect to the bolt head. This likely led to some variability in how directly axial the applied tensile load was.

In the machined samples, the stress profile develops slightly quicker and yielding and ultimate failure both occur at smaller amounts of strain than in the unmodified samples. This may be because a stress concentrating artificial neck in the shaft of the bolt is introduced by the machining. The machined samples, in general, have wider spread in the data, both in terms of the value of stress at a particular amount of strain as well as the location on the strain axis where yielding and ultimate failure occur. Because of this, the averaged stress curve for machined samples seems not to exhibit the typical “shoulder” after yielding that is expected in tensile test samples. Inspection of the individual sample data will show that this shoulder is present, yet less pronounced than in the unmodified samples and is likely convoluted by the spread in the stress-strain data.

Regarding the machined samples, the increased spread in the data can likely be attributed to the removal of the threads. The cold working process of rolling the threads will tend to compress and refine the crystal structure of the outer material. Similarly,

during the quenching portion of the heat treatment process the outer material grains are cooled faster than the inner grains. This can lead to a radial gradient of material hardness. Perhaps these two actions also lead to a more regular crystal structure. For the 3/8-16 bolts studied, the portion of the material with a more regular crystal structure would account for roughly 30% of the cross section. Effectively, removing the threads from a portion of the bolt leaves a portion of the bolt where the less controlled properties of the raw “medium carbon steel” drawn wire govern.

The nuts were compressed until they plastically deformed to roughly half their original height. An example of one tested sample is shown next to a fresh sample for comparison in Figure 2-12. The compression data for the nuts were processed to isolate the portion of data concerning deformation of the conical washer. An example of the total test curve of load against deformation is presented in Figure 2-13.

Figure 2-12. Before and After Comparison of Compressed Nut Sample.

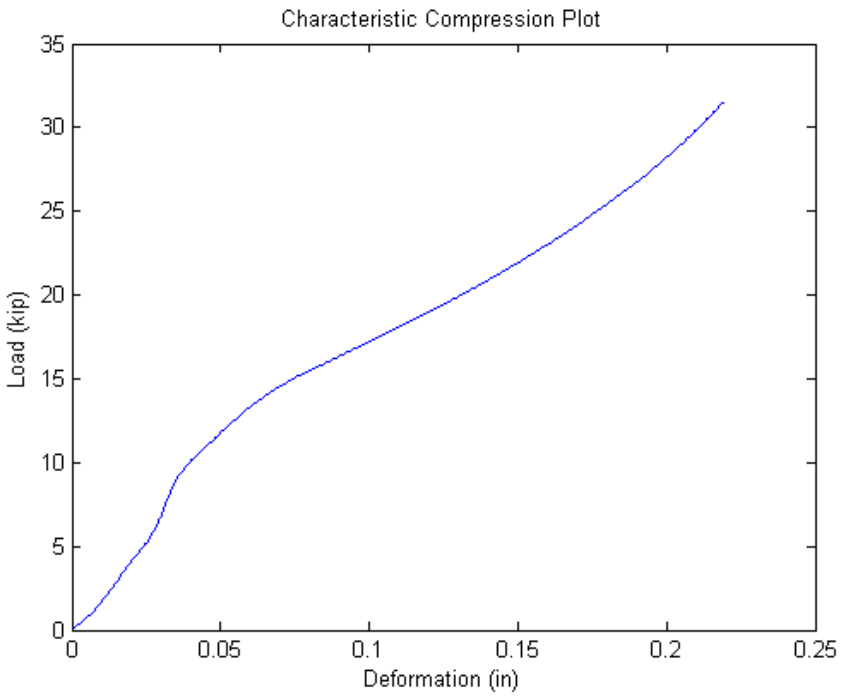

Figure 2-13. Characteristic Total Sample Compression Plot.

In this figure it can be seen that there is steep increase in the data around 7 kiloPounds and 0.035 inches of deformation. Previous to this point, only the washer is being compressed. This corresponds to nominal height of the washer. The increased steepness of the curve between 7 and 10 kiloPounds, is likely due to encountering the thin swaged flange which joins the nut and washer. Since this material is cold formed it will have a locally refined grain structure and higher strength. At around 10 kiloPounds and 0.04 inches of deformation there is a shoulder. This is where the entire nut and washer assembly is being elastically compressed. At around 15 kiloPounds and 0.07 inches deformation there is a second shoulder, indicating the onset of plastic deformation, and the curve takes an exponential shape, indicating increasing strength of the material as it is being compressed.

2.2 Load Cell Calibration

2.2.1 Load Cell Set-Up

The bolt used as a load cell was modified as described in Section 2.1.1. The bolt then had strain gauges applied in a half-bridge configuration as described in Figure 2-14 using the procedure listed in the installation instructions provided by Vishay Precision Gauges [37]. The strain gauges are shown in an artificial color and out of scale for diagrammatic purposes. Note that the strain gauges are installed diametrically opposed in the center of the gauging region of the load cell and with the wire solder pads in the same orientation with respect to the bolt head. The strain gauge configuration reflects item number 5 in Table 2-3 [38]. This configuration was chosen due to the small amount of space available for mounting strain gauges on the bolts. A second bolt was set-up with the same half-bridge configuration in order to complete the bridge for testing. A second bolt with strain gauges was chosen as a bridge completion unit because this allows for temperature compensation in future testing of the splice joint under load. Temperature compensation is not provided if constant value resistors are used to complete the bridge. The strain gauges used are Micro-Measurements General Purpose Strain Gauges (distributed by Vishay Precision Gauges) model number EA-06-060LZ-120/E. The selected strain gauges have a nominal grid resistance of 120 Ohms with a tolerance of plus-or-minus 0.3%.

Table 2-3. Table of Strain Gauge Configurations.

1

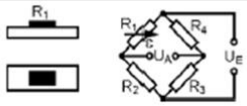

$$\varepsilon = \varepsilon_n + \varepsilon_b = \frac{4}{k} \cdot \frac{U_A}{U_E} - \varepsilon_S$$

T	F_N	M_b	M_d
1	1	1	0

2

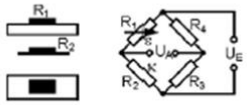

$$\varepsilon = \varepsilon_n + \varepsilon_b = \frac{4}{k} \cdot \frac{U_A}{U_E}$$

T	F_N	M_b	M_d
0	1	1	0

3

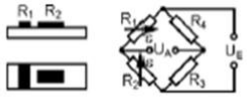

$$\varepsilon = \varepsilon_n + \varepsilon_b = \frac{1}{(1+\mu)} \cdot \frac{4}{k} \cdot \frac{U_A}{U_E}$$

T	F_N	M_b	M_d
0	1+υ	1+μ	0

4

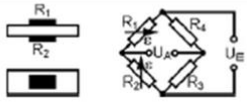

$$\varepsilon = \varepsilon_b = \frac{1}{2} \cdot \frac{4}{k} \cdot \frac{U_A}{U_E}$$

T	F_N	M_b	M_d
0	0	2	0

5

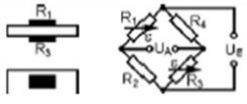

$$\varepsilon = \varepsilon_n = \frac{1}{2} \cdot \frac{4}{k} \cdot \frac{U_A}{U_E} - \varepsilon_S$$

T	F_N	M_b	M_d
2	2	0	0

6

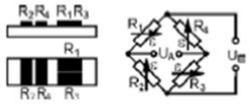

$$\varepsilon = \varepsilon_n + \varepsilon_b = \frac{1}{2(1+\nu)} \cdot \frac{4}{k} \cdot \frac{U_A}{U_E}$$

T	F_N	M_b	M_d
0	2(1+υ)	2(1+υ)	0

7

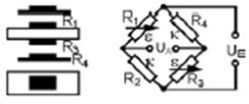

$$\varepsilon = \varepsilon_n = \frac{1}{2} \cdot \frac{4}{k} \cdot \frac{U_A}{U_E}$$

T	F_N	M_b	M_d
0	2	0	0

8

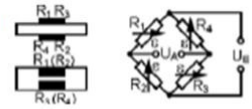

$$\varepsilon = \varepsilon b = \frac{1}{2} \cdot \frac{4}{k} \cdot \frac{U_A}{U_E}$$

T	F_N	M_b	M_d
0	0	4	0

9

$$\varepsilon = \varepsilon_n = \frac{1}{2(1+\mu)} \cdot \frac{4}{k} \cdot \frac{U_A}{U_E}$$

T	F_N	M_b	M_d
0	2(1+υ)	0	0

10

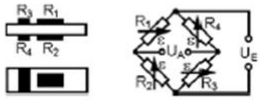

$$\varepsilon = \varepsilon_b = \frac{1}{2(1-\mu)} \cdot \frac{4}{k} \cdot \frac{U_A}{U_E}$$

T	F_N	M_b	M_d
0	0	2(1+υ)	0

11

$$\varepsilon = \varepsilon_b = \frac{1}{2(1+\mu)} \cdot \frac{4}{k} \cdot \frac{U_A}{U_E}$$

T	F_N	M_b	M_d
0	0	2(1+υ)	0

12

$$\varepsilon = \varepsilon_b = \frac{1}{2} \cdot \frac{4}{k} \cdot \frac{U_A}{U_E}$$

T	F_N	M_b	M_d
0	0	2	0

13

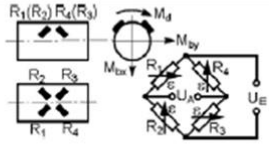

$$\varepsilon = \varepsilon d = \frac{1}{4} \cdot \frac{4}{k} \cdot \frac{U_A}{U_E}$$

T	F_N	M_{bx}	M_{by}	M_d
0	0	0	0	4

14

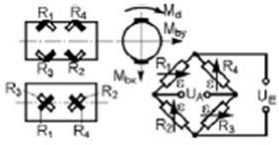

$$\varepsilon = \varepsilon_d = \frac{1}{4} \cdot \frac{4}{k} \cdot \frac{U_A}{U_E}$$

Tt	F_N	M_{bx}	M_{by}	M_d
0	0	0	0	4

15

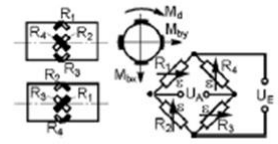

$$\varepsilon = \varepsilon_d = \frac{1}{4} \cdot \frac{4}{k} \cdot \frac{U_A}{U_E}$$

t	F_N	M_{bx}	M_{by}	M_d
0	0	0	0	4

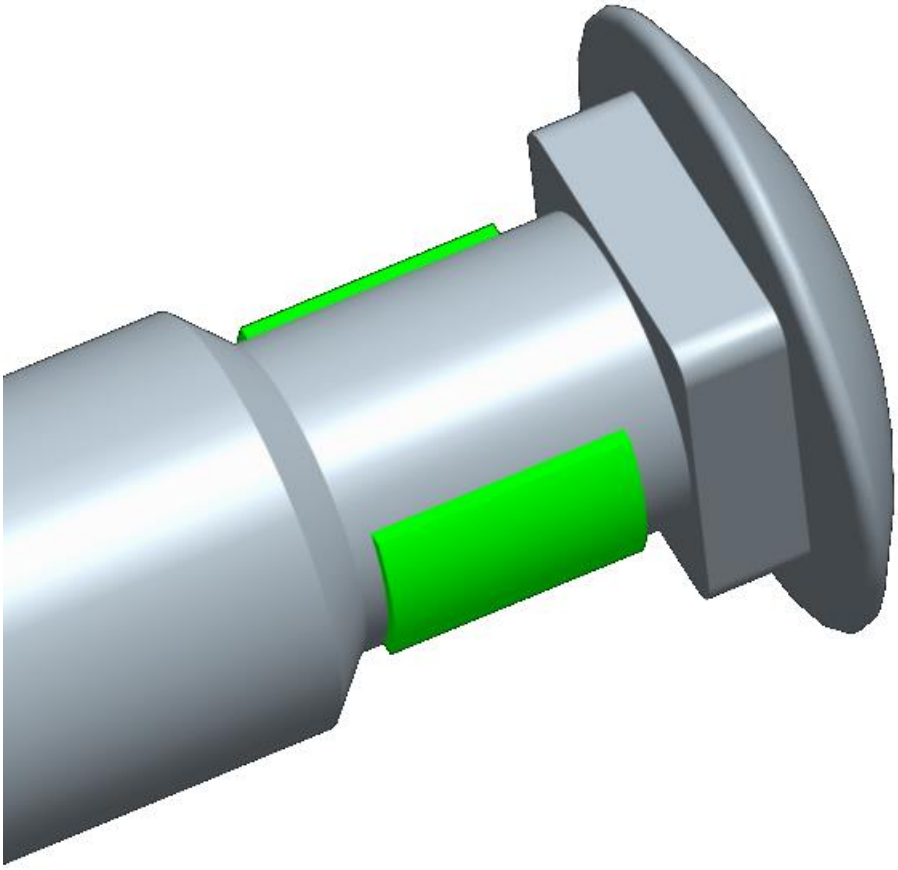

Figure 2-14. Strain Gauge Configuration.

A DATAQ Instruments data logger (Model Number D170-ULS) was used for measurement of strain data from the load cell [39]. The data logger has 8 differential voltage inputs with a measurement tolerance of plus-or-minus 50 microVolts. This tolerance was neglected in the analysis provided that the measured voltage variation data tended to be on the order of one hundred times larger than the voltage tolerance. The total calibration system is shown in Figure 2-15. A sample detail is shown in Figure 2-16.

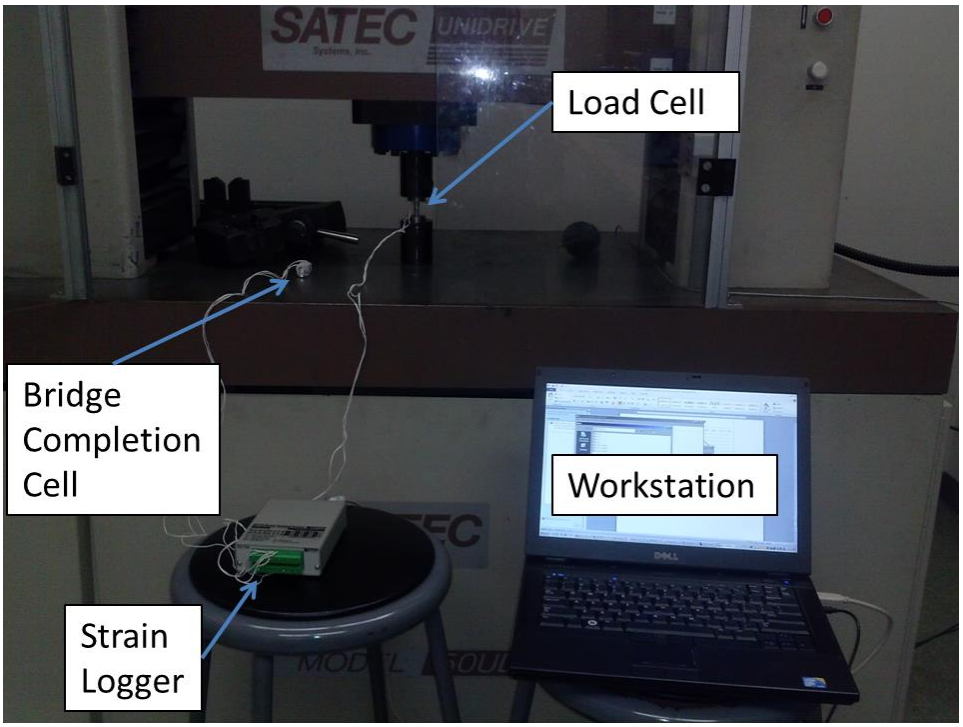

Figure 2-15. Load Cell Calibration Set-Up.

Figure 2-16. Detail View of Load Cell in Grips.

2.2.2 Calibration Procedure

The load cell was calibrated by applying a tensile load to the load cell with the SATEC tensile testing machine at constant pull rate of 0.01 inches per minute while the change in voltage across the strain gauge half bridge was measured using the D170-ULS data logger. The load was applied until a maximum tensile load of 2000 pounds was reached in the load cell. Both sets of data were manually processed to eliminate the settling period and to align the peaks of change in voltage and applied load. In Figure 2-17 both sets of data are shown in normalized format in order to provide a description of the shape of the plots.

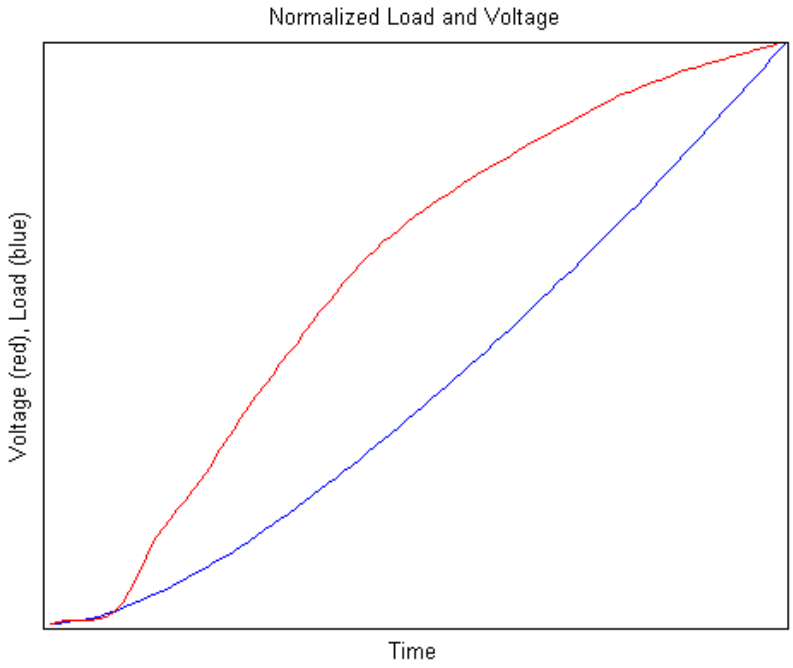

Figure 2-17. Change in Voltage Plotted Against Load Applied to Load Cell.

The SATEC tensile testing machine dwelled (ceased increasing load) at the maximum of load application. By taking the slope between the values of change in voltage and load at this point and at the onset of loading, a linear calibration function was determined and is shown in Equation 2-1, with P indicating applied load and V indicating change in voltage across the strain gauge bridge.

$$P = (V * 2 * 10^6) - 0.24 \quad (2\text{-}1)$$

2.3 Experiment

2.3.1 Set-Up and Procedure

The basic premise of this experimentation was to apply known values of torque to a nut on the load cell's threads while the load cell was clamping two pieces of material mounted in a vice. The DATAQ D170-ULS data logger was used to collect change in voltage data from the load cell strain gauge bridge as torque was applied. The calibration curve was then applied to the collected data. The total set-up is shown in Figure 2-18 while a sample detail is shown in Figure 2-19.

A random sampling of 20 nuts as described in Section 2.1.1 was used throughout the experiment. Before testing, a 3/8"-16 tap was passed through each nut in order to ensure that the surfaces of the threads were clean and uniform. This should also reduce the likelihood of the coefficient of friction of the threads to change with each tightening-loosening procedure. The threads of the load cell were similarly treated with a 3/8"-16 die.

A calibrated FUTEK Advanced Sensor Technology digital torque wrench (Model Number TAT500) and Sensotec torque data logger (Model Number SC2000) were employed to ensure accurate and repeatable applications of torque.

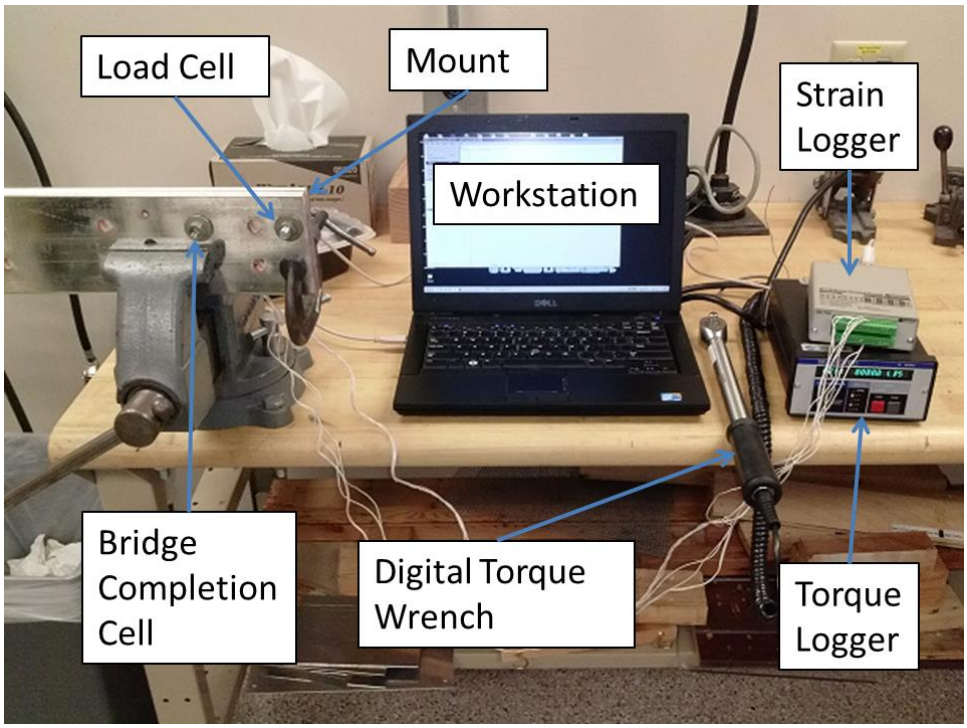

Figure 2-18. Torque-Pretension Correlation Set-Up.

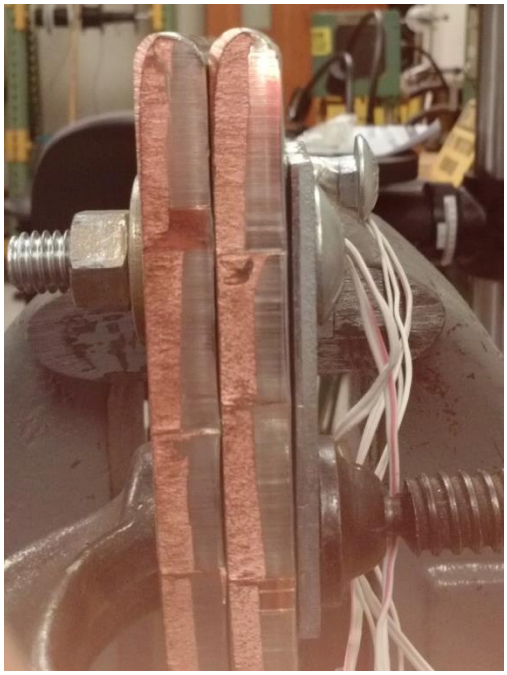

Figure 2-19. Detail of Mounted Load Cell and Saddle.

The load cell was mounted to two pieces of copper bus bar described in Section 1.2.3. The bus bar has holes punched through it for the purpose of creating bolted splice joints. From this point on in this chapter, this material will be referred to as the mount. The load cell was driven through a saddle which typically carries two carriage bolts. The saddle has square holes which hold the square portion of the carriage bolt shaft in order restrain them from rotating. The unused portion of the saddle was clamped to the mount. The CAD model in Figure 2-20 describes this set-up.

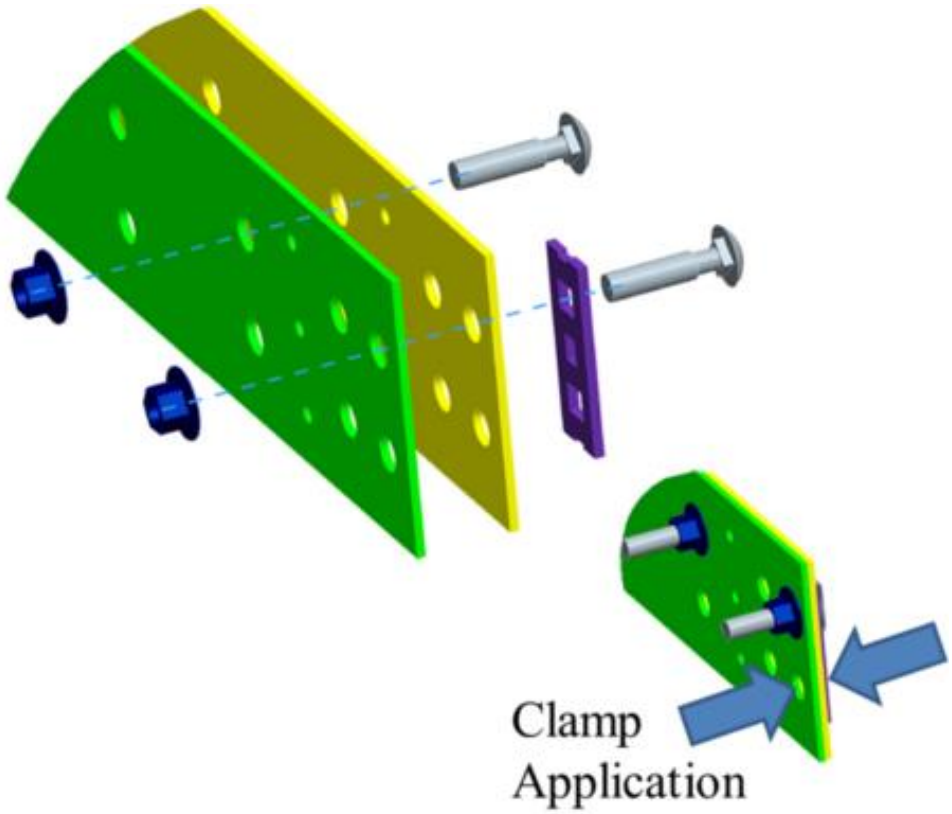

Figure 2-20. Assembly Diagram of Torque-Pretension Correlation Set-up.

The bridge completion cell was rested in another hole in the mount with a nut threaded onto it such that there was no tension load applied to the cell. This was done to keep the bridge completion cell steady during testing.

A nut was randomly selected from the grouping of 20 nuts with treated threads. This nut was threaded onto the load cell and turned by hand until it could no longer be turned without much effort. Since this was a subjective process, the data stream was examined simultaneously in order to ensure that there was no load applied to the load cell before torqueing began with the torque wrench. At this point, the torque wrench was used to apply torque to the desired value while the D170-ULS data logger collected data from the load cell. The nut was then removed with an open-end wrench and returned to the pool of

nuts. This procedure was repeated 10 times each at torque values of 50, 100, 150, 200, and 250 pounds-inch.

2.3.2 Experiment Data

Since the change in voltage data were collected from the load cell in a continuous stream, the data were manually processed to isolate portions of data when the load cell was in a steady load state after torque application and immediate settling. Figure 2-21 motivates the necessity for this processing.

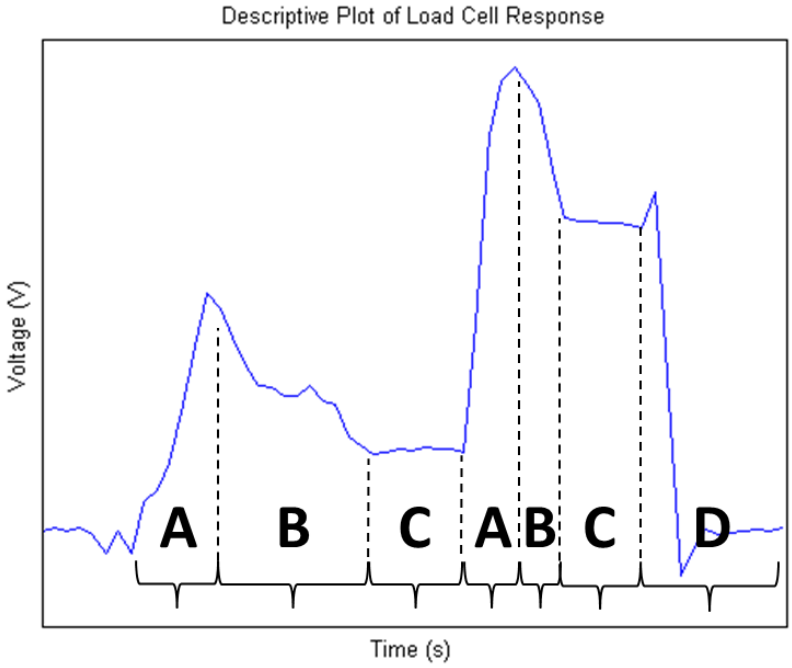

Figure 2-21. Descriptive Plot of Load Cell Voltage Response to Applied Torque.

This figure is a descriptive plot of the voltage response of the load cell during two successive applications of metered torque to the nut followed by the removal of the nut.

There are 4 primary response regions of the measured signal. Region A, or the application region, is the region in which torque is applied. The amount of load in the bolt is reported as especially high during torque application because no torque measurement strain gauges are on the cell and thus the torque portion of the applied load cannot be filtered out. In region B the load is removed and the load cell settles to a steady load state condition, region C. Region C is the area of interest and is where the bolt pretension measurements are made. Pretension measurements are an average of this entire region for a given torque application trial. Region D is the release and ambience region. It can be seen that there is a sharp increase in voltage at the onset of the release region. This is because the bolt will twist slightly as static friction is overcome in the system and the nut can freely rotate off.

2.4 Experimental Results and Discussion

The mean experimental load cell measurements are plotted against applied torque in Figure 2-22. Standard deviation is included in this plot. By evaluation of the deviation envelope it can be seen that as the applied torque increases, the data become more consistent. The change in voltage tends to increase linearly with applied torque. A linear fit line (Equation 2-2) is plotted with the data. The linear fit line has a coefficient of determination of 0.9561.

$$V = 7 * 10^{-6}T + 0.0003 \quad (2\text{-}2)$$

In Equation 2-2, V indicates the change in voltage and T indicates the applied torque.

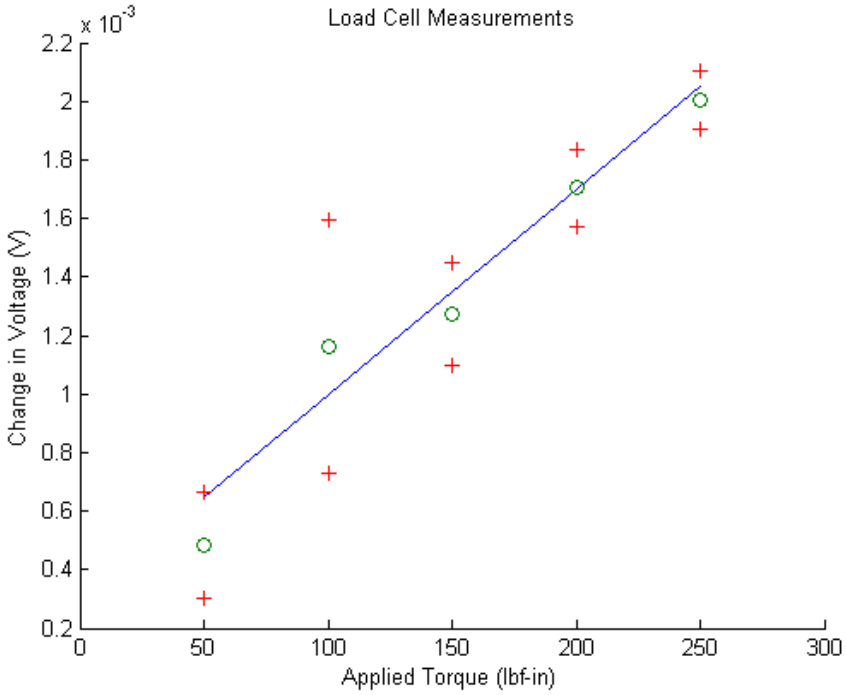

Figure 2-22. Mean Change in Voltage Values (o) Plotted with Standard Deviation (+) and Linear Fit Line.

Several factors could cause the trend to decrease the standard deviation of change in voltage at a given applied torque as applied torque is increased. At present, the most reasonable explanation for this behavior is that at the lower applied torques the magnitude of the measurement accuracy tolerance of the torque wrench is closer to the magnitude of the measured torque than at higher torque applications. This reasoning stands for the measurements collected from the strain gauges as well.

The data from Figure 2-22 are tabulated in Table 2-4. In Table 2-5 the experimentally determined calibration is applied and tabulated along with theoretical

loads determined using the Equation 2-3 [40] as well as percent error between the experimental values and the theoretical values.

$$P = \frac{T}{KD} \tag{2-3}$$

In this equation, T indicates the applied torque, P indicates the bolt pretension, D is the major diameter of the bolt threads, and K is an empirical constant. For the case of a steel nut on a steel bolt with clean, dry threads, the value of K is assumed to be 0.20.

Table 2-4. Experimental Response to Applied Torque Data

Applied Torque (lbf-in)		50	100	150	200	250
Change in Voltage (mV)	**Mean**	0.483	1.163	1.271	1.704	2.004
	StDev	0.180	0.431	0.176	0.133	0.099

Table 2-5. Bolt Pretension Prediction using Linear Calibration.

Applied Torque (lbf-in)	50	100	150	200	250
Experimental Mean Bolt Pretension (lbf)	967	2326	2542	3407	4008
Deviation of Pretension (lbf)	359	862	352	266	197
Theoretical Bolt Pretension (lbf)	667	1333	2000	2667	3333
Percent Error (%)	44.98	74.49	27.10	27.75	20.25

It is important to note that the use of the empirical constant in Equation 2-3 produces a deterministic theoretical value that is, in reality, highly probabilistic due to the nature of friction between dry surfaces. When bolt pretension is a primary design parameter, either the value of K should be evaluated on a case by case basis, or a process specific modeling equation should be determined.

The calibration of the load cell was validated with a Honeywell Model DT Thru-Hole Load Cell. This load cell has a compressive load range of 7500 pounds and accuracy of plus or minus 75 pounds. The validation apparatus is shown in Figure 2-23.

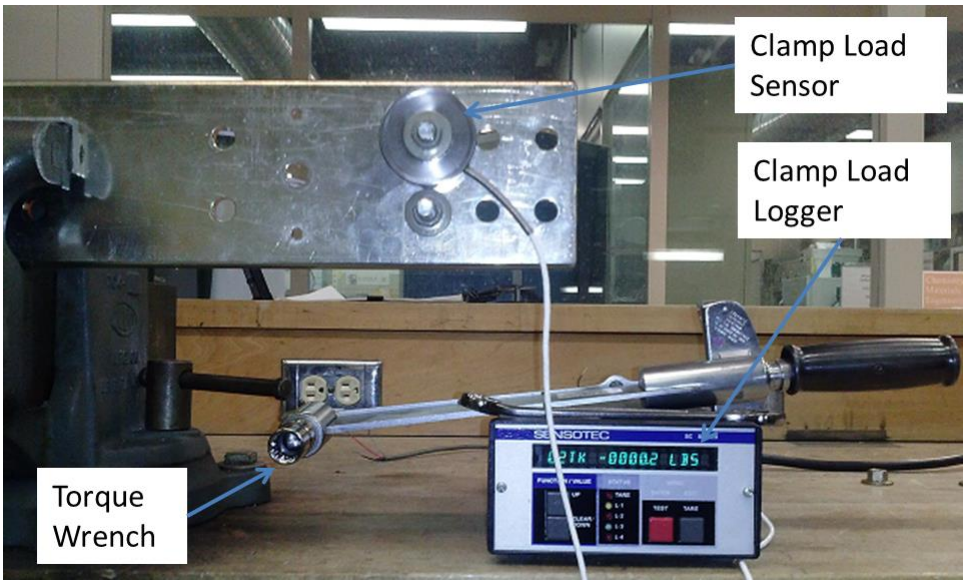

Figure 2-23. Load Cell Validation Set-Up.

The mounting and procedure for the validation were the same as for the experiment. The experimental load cell was mounted in the saddle on the mount material. The Thru-

Hole load cell was place between the nut and the mount. Torque was applied for 10 trials each of metered torque at 50, 100, 150, 200, 250 and 350 pounds-inch. A manual torque wrench was used because the Thru-Hole load cell required the use of the Sensotec data logger. The averages of collected pretension data for each set of trials are shown along with the experimental values measured with the load cell in Table 2-6.

Table 2-6. Comparison of Experimental and Validation Pretension Values.

Applied Torque (lbf-in)	50	100	150	200	250
Experimental (lbf)	967	2326	2542	3407	4008
Validation (lbf)	387	676	955	1196	1456
Percent Error (%)	149.87	244.08	166.17	184.87	175.27

From examination of data in the Table 2-6 it can be seen that for each applied torque the mean validation pretension value is roughly 1/3 that measured with the experimental load cell. Noting this, a correlating factor of 1/3 is introduced to the calibration equation, Equation 2-2. The final calibration equation is presented in Equation 2-4. Comparison of the experimental data computed with Equation 2-4 and the validation data are presented in the Table 2-7. Also, in this table a value of pretension as a result of one trial application of 350 pounds-inch is computed using Equation 2-4 and is compared with the pretension value measured with the validation load cell.

$$P = (1/3)[(V * 2 * 10^6) - 0.24] \quad (2\text{-}4)$$

As in Equation 2-2, P indicates the pretension load and V indicates the change in voltage.

Table 2-7. Corrected Experimental Pretension Values and Validation Values with Percent Error.

Applied Torque (lbf-in)	50	100	150	200	250	350
Experiment (lbf)	322	775	847	1136	1336	1833
Validation (lbf)	387	676	955	1196	1456	2028
Percent Error (%)	16.64	14.77	11.24	5.00	8.25	9.62

Upon examination of percent error data presented in Table 2-7 it can be seen that the modification to the calibration equation provides for an experimental load cell which can be use with good confidence for *in-situ* measurement and experimentation.

Plotting the measured pretension load using calibration Equation 2-4 against the applied torque and applying a linear curve fit provides a modeling equation, Equation 2-5, for predicting the pretension load in the bolt for a given applied torque. This is shown in Figure 2-23. The fit line has a coefficient of determination of 0.9562. Validation measurements made with the industry clamping load cell are shown for comparison.

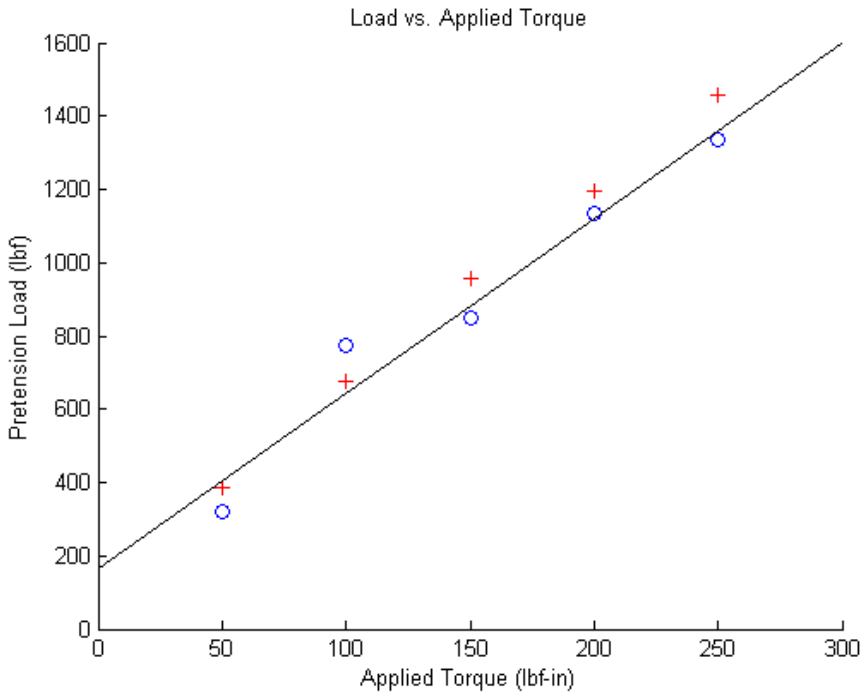

Figure 2-24. Experimental (o) and Validation (+) Loads against Applied Torque.

$$P = 4.778T + 166.5 \quad (2\text{-}5)$$

In Equation 2-5 P is the modeled pretension load and T is the applied torque. It is proposed that this equation can be used to model pretension in Grade 5 3/8-16 UNC 2A bolts in the specific application of clamping two pieces of 0.25 inches nominal thickness tin plated copper bus bar with a 3/8-16 steel washer with integral conical washer. The threads of both bolt and nut must unlubricated. The value computed, using Equation 2-5, at 350 pounds-inch is compared with the value measured with the experimental load cell as well as the value measured using the industry clamping load cell in Table 2-8.

Table 2-8. Comparing Experimental, Validation, and Modeled Pretension Load.

Pretension Load at 350lbf-in		
Experimental	**Validation**	**Model**
1833	2028	1839

The modeled value of pretension is very similar to the value measured experimentally with the load cell. Regarding the value measured with the industry clamping load cell the model has a percent error of 9.3%.

Overall, it is apparent that the experimental load cell can produce accurate measurements of bolt pretension. Furthermore, using Equation 2-5, one can model the pretension load for the system of interest. It is important to note that the model will fail at values of applied torque lower than 50 pounds-inch as it predicts 166.5 pounds of pretension load with no torque applied to the system. This is acceptable in the present study because the nominal applied torque for this system is 350 pounds-inch. Further study could include the onset of pretension at small amounts of torque and improve the quality of the model with a piece-wise calibration curve and pretension model. The accuracy of the model would also be improved by testing more samples and more trials at each value of applied torque. It is also of interest to re-iterate that the theoretical calculation of Equation 2-3 will over-predict the pretension load by at least 150%. In a design problem where optimal performance of the clamp under mechanical load was critical, use of this calculation could lead to failure of the design.

CHAPTER 3: Electrical Resistance as a Function of Bolt Pretension

Due to increases in electrical resistance at the point of splicing in a power distribution network, this is where Joule heat generation is of primary concern. This is a function of the material properties and mechanical quality of the surfaces in contact, as well as the contact pressure due to pretension in the bolt. Section 3.1 describes an experiment for evaluating the variation of electrical resistance of the bolted splice joint with respect to applied torque/bolt pretension. Section 3.2 describes a numerical simulation to describe the contact pressure profile in the joint.

3.1 Electrical Resistance in the Surface Contact Zone

3.1.1 Experimental Approach

New samples of bus bar material were spliced together using a pair of 3/8-16 carriage bolts, bolt saddle, and 3/8-16 nut with integral conical washer. The resistance across the joint was measured with a Biddle Ohmmeter. The probes of the Ohmmeter were placed, one on each side of the splice joint, 0.5 inches from the splice. Metered torque was applied to the intended value on one bolt, then to the other bolt. Although this may cause irregular settling of the clamped surfaces, this torqueing method was used because this is the practice in the field. A CAD model showing assembly of the test specimen is shown in Figure 3-1. The total experiment set-up is shown in Figure 3-2.

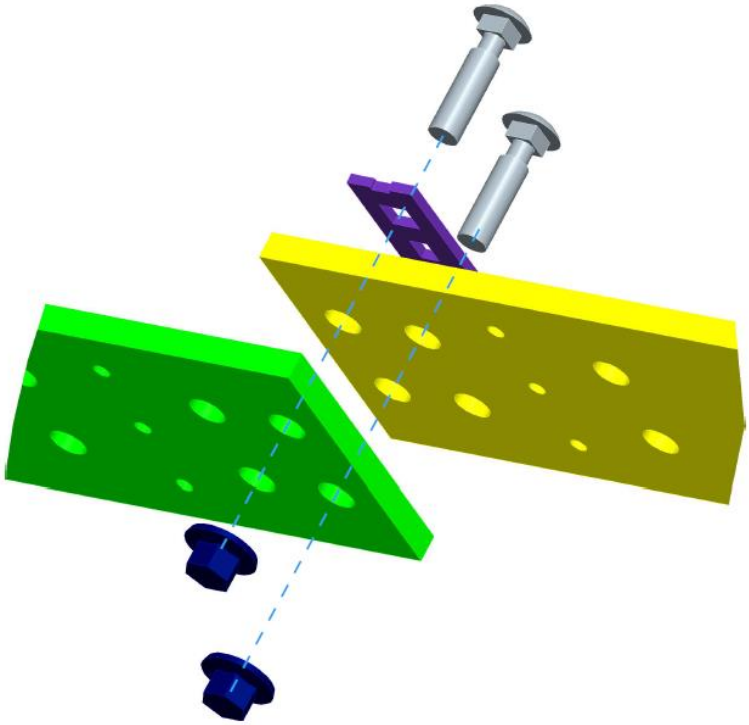

Figure 3-1. CAD Model of Resistance Measurement Assembly.

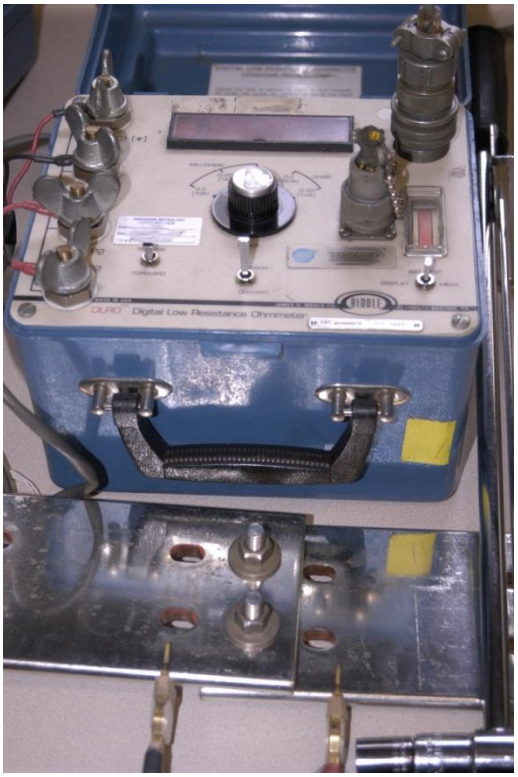

Figure 3-2. Resistance Measurement Experiment Set-Up.

3.1.2 Results

The resistance data for the experiment are presented in Table 3-1 and are plotted in Figure 3-3. In Table 3-1 and Figure 3-3, the contact resistance datum indicated at zero pounds-inch of applied torque corresponds to the point at which torque can no longer be applied to the nut with the fingers.

Table 3-1. Resistance across the Splice.

Contact Resistance (mΩ)	0.054	0.029	0.005	0.004	0.0035	0.003
Applied Torque (lbf-in)	0	3	9	12	18	48

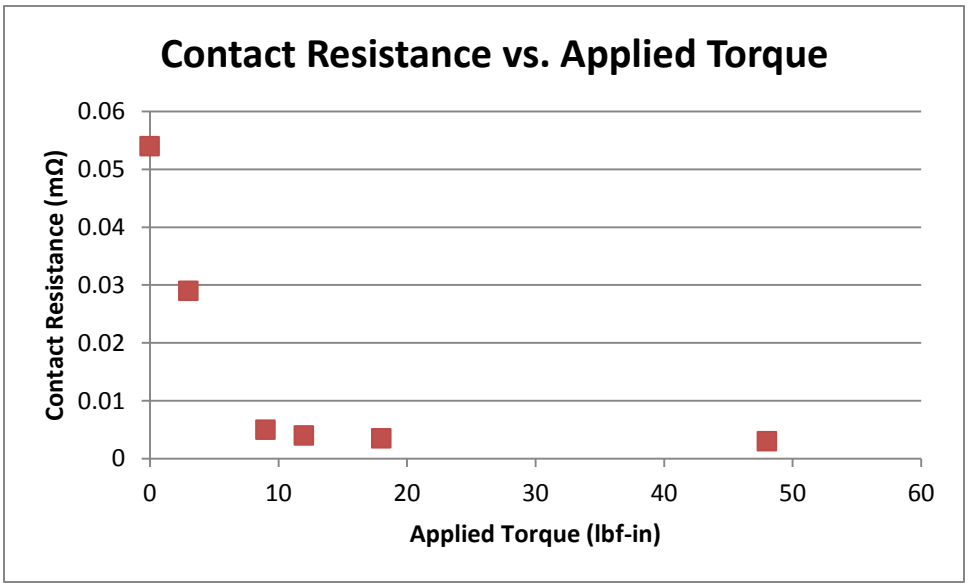

Figure 3-3. Plot of Resistance across the Splice.

3.1.3 Discussion

The resistance across the splice quickly falls off asymptotically as clamp load is increased. The change in resistance across the splice for brand new bus material seems to asymptotically approach 0.003 milliOhms as applied torque is increased. Qualitatively, these data have a trend similar to contact resistance computed as a function of the applied load for the Weierstrass profile [41], as well as experimental contact resistance data and computed contact resistance values for a cluster of a-spots as presented by Braunovic et al. [30].

The resistivity of the copper base material is temperature dependent [42]. Since Joule heating of the splice will take place when the bus has a current load applied, measurements of the contact resistance should be made while current is applied to get a more complete understanding of the behavior. Furthermore, the geometry of the bus bar will also change in time due to thermal expansion. This may influence the contact resistance by redistributing the locations of surface asperities on either contact surface. For relatively clean samples with good quality surfaces, it may be that problematic localized heating arises as a function of stress relaxation of the bolts which provide clamping load to the splice. The Joule heating model for conductors carrying current is given by Equation 3-1 [43].

$$\dot{q} = I^2 R \tag{3-1}$$

In this equation, $\dot{q}$ is the heat generated in the conductor, I is the applied current, and R is resistance. In the reported resistance measurements there is a 17 times increase in resistance across the splice when the pretension is negligible. It can be clearly seen that

loss of pretension in the bolt due to transient relaxation of the bolt material is a probably root cause for localized heating of the splice. Data on the creep behavior medium carbon steels is not forthcoming in the literature. As such, further analysis is not provided.

3.2 Qualitative Prediction of Contact Pressure

3.2.1 Numerical Simulation

The finite elements method was used to simulate the bolted joint and provide a descriptive view of the contact pressure profile between the mating conductive surfaces of the bus sections. All simulations were implemented in ANSYS v.13.0. A two-dimensional study was conducted assuming perfectly planar bus bar. The nominal dimensions for the bus bar, bolt, and nut were used. The pretension is modeled from Equation 2-5 for the nominal torque of 350 pounds-inch. The modeled value of pretension was reduced to 2 significant figures for a value of 1800 pounds at each bolt. The loading was applied as a distributed load on the surfaces where the bolt head and conical washer nominally interface with the bus. Plane183 8-node planar solid elements were used to model the bus. A modulus of elasticity of 17,000,000 pounds per square inch and Poisson's ratio of 0.3 were used to model the copper material. Frictionless contact between the two sections of the bus bar was modeled using Contact172 and Target169 elements. To avoid rigid motion, the lower bus bar is constrained at two points in both x- and y- directions while the upper bus bar is constrained in the x-direction. The set-up for the simulation is shown in Figure 3-4.

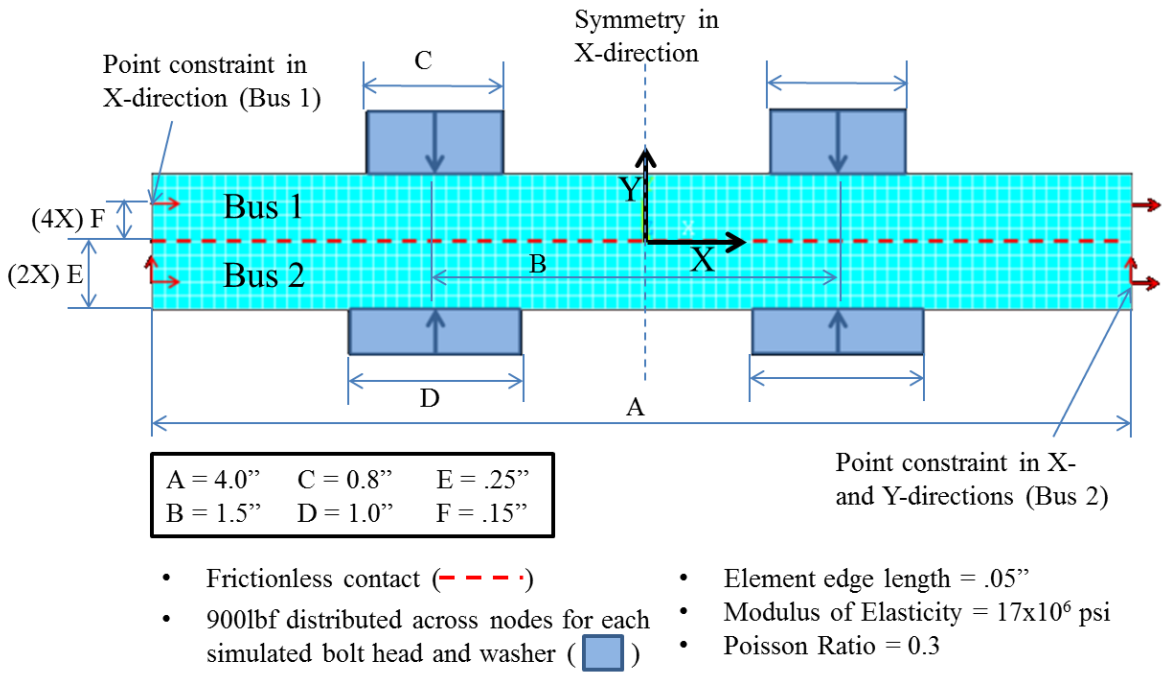

Figure 3-4. Schematic for 2D Contact Simulation.

3.2.2 Results

The qualitative two-dimensional contact pressure map for simulated contact between perfectly planar bus bars is presented in Figure 3-5. The qualitative map of von Mises stress is presented in Figure 3-6.

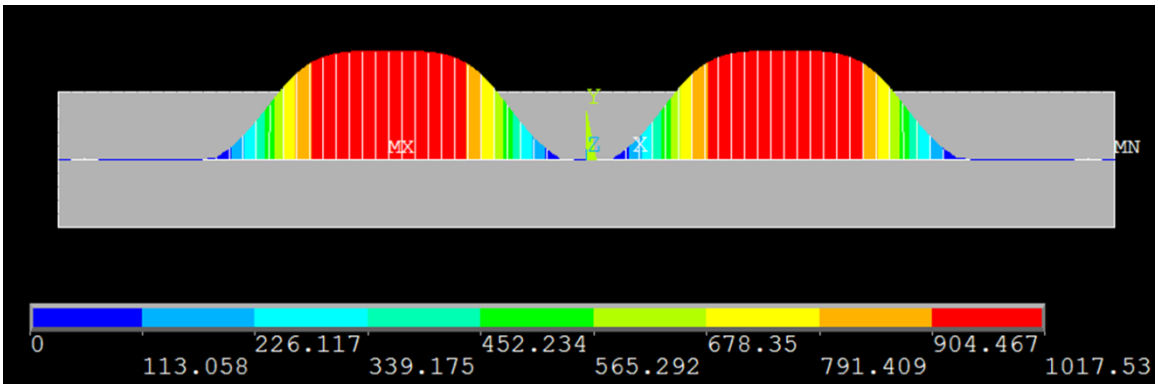

Figure 3-5. Descriptive Contact Pressure Plot.

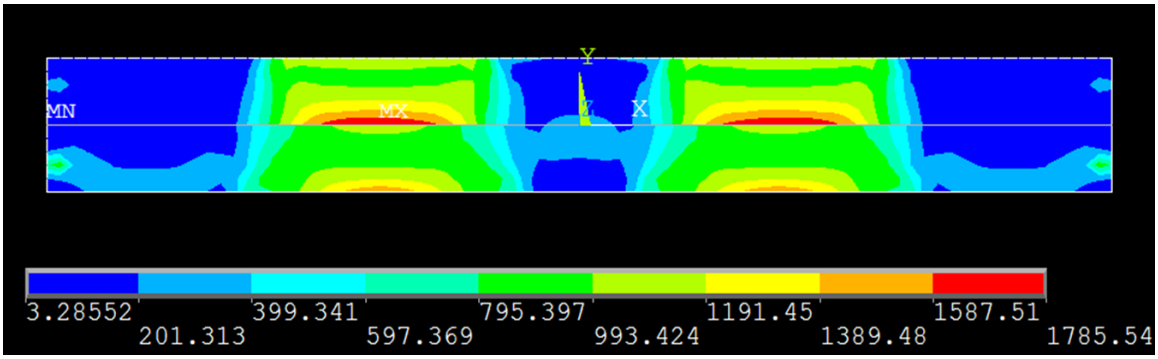

Figure 3-6. Descriptive von Mises Stress Profile.

3.2.2 Discussion

In Figure 3-5 it can be seen that, for perfectly planar surfaces, the contact pressure is focused at the location of clamp loading and quickly falls off to be negligible outside of the direct area of influence under the bolt head and washer system. This observation is supported by the plot of von Mises stress, in Figure 3-6, which shows that the material is primarily stressed in the area that is directly influenced by the clamping of the bolt. The local stresses on the extremities of the bus bar are phantoms due to the modeled displacement constraint at these locations.

The simulation is idealized to solve for the case of perfectly planar mating surfaces. It will be seen that this is not realistic. On the other hand, comparison of these results with real samples of disassembled bus can provide insight into the nature of contact pressure and internal stresses in the bus. Macro photographs are presented which show the mating surfaces of previously in-use bus material. Via examination of contact witness marks, one can determine where a mating surface has actually come into contact with other mating surfaces. In Figure 3-7, one mating surface of a power conducting bus is shown. In Figure 3-8 and 3-9 the mating surfaces of a power conducting bus and load bus

are shown, respectively. The load bus is bolted to the power conducting bus for distribution of current to individual loads.

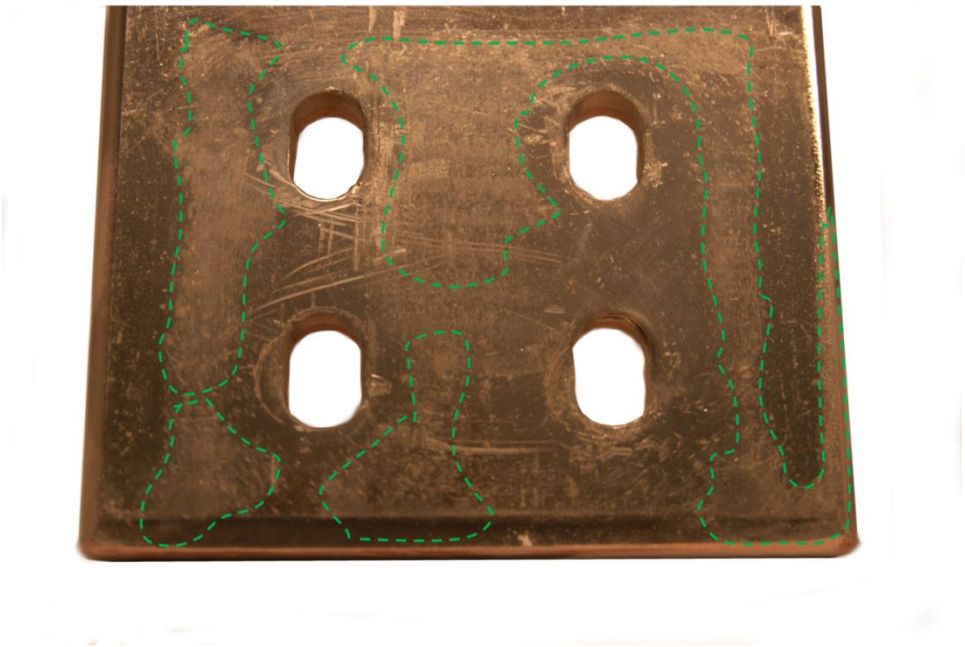

Figure 3-7. Mating Surface of Power Conducting Bus with Witness Marks Outlined.

Figure 3-8. Mating Surface where Power Conducting Bus meets Load Bus

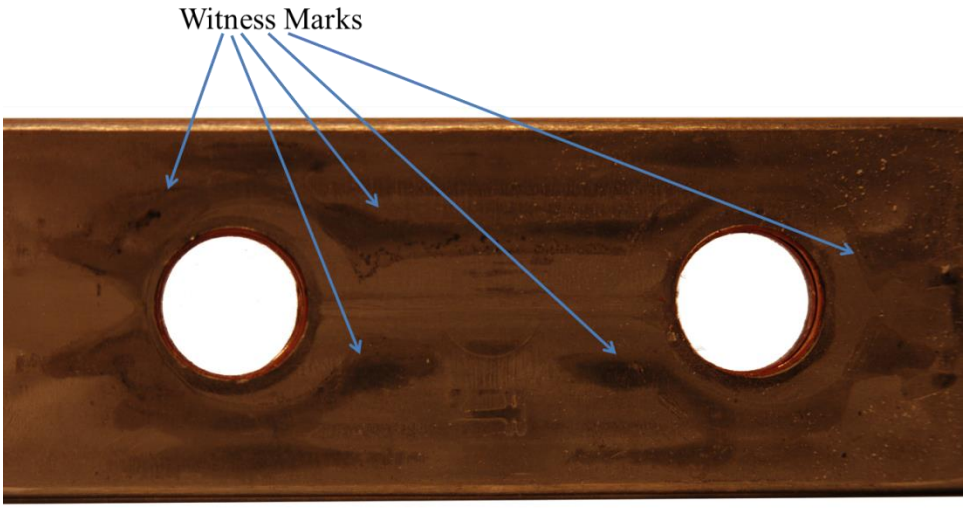

Figure 3-9. Mating Surface of Load Bus.

From all of the Figures 3-7 through 3-9, the first thing to note is that the true mating surface is much smaller than the expected or “apparent” mating surface. For example, in

Figure 3-7, the green dashed line shows the rough outline of the witness mark left by contact with another piece of bus bar. The location shown in Figure 3-7 is where this piece of main power conducting bus bar would be spliced to a second piece of main power conducting bus bar. Figures 3-8 and 3-9 show the reciprocal mating surfaces of a main power conducting bus and load bus. Again it can be noted that the actual contact area is much smaller than the apparent contact area. In the case of

Figure 3-7, the irregular shape of the actual mating area is a function of geometric tolerances in the cross section of the bulk copper material with respect to its length and potentially process tolerance allowance for the thickness of the tin plating. The influence of these effects is seen in both mating surfaces, adding to the uncertainty of the problem. In Figures 3-8 and 3-9 the shape of the contact area is primarily a function of the construction method of the load bus. This particular load bus is a hollow copper bar which is cold formed in a press to create the flat mating surface and punch the mounting holes. Flattening of the originally tubular material leaves macro-scale surface waviness in the mating surface. The irregular pattern of contacting surfaces results and is not designed for.

In the finite elements analysis, the mating surfaces are treated as perfectly planar. As such, their deformation under the clamping load of the simulated bolt system leads to a situation in which the surfaces come into contact directly in between the bolt head and washer. This leads to internal stresses being concentrated around this point.

Examination of the samples shows that, without further quantifying study to produce accurate surface models, the qualities of the real situation must be extrapolated by interpretation of the simulation results because the bus bars are not perfectly planar. The

material shows contact wear outside of the area predicted in the simulation. In the case of main power conducting bus, this is probably due to combination of the geometric tolerance on the cross section of the bar as well as additional deformation of the area surrounding splicing holes as the holes are punched cold. Based on the simulation results, the contact pressure is expected to be concentrated in the areas showing witness marks and to quickly fall off on the fringes of these areas. Internal stresses in the material are generated due to the constraint created by the clamping bolts as well as interfacial contact. The areas where contact pressure is concentrated are where the conduction of electricity occurs across the splice.

Splicing occurs at numerous points in the power distribution system. Every individual load gets its power from a load bus which is bolted to the main power bus. Every splice between main power bus sections is a double lap joint which uses a small splicing patch of copper bus bar material to complete the splice. This is described in Figure 3-10. As such, the actual number of interfaces is twice the number of such splice locations. For the power application of study, three-phase power is used. This then triples the amount of splicing interfaces for each point along the current stream of the bus.

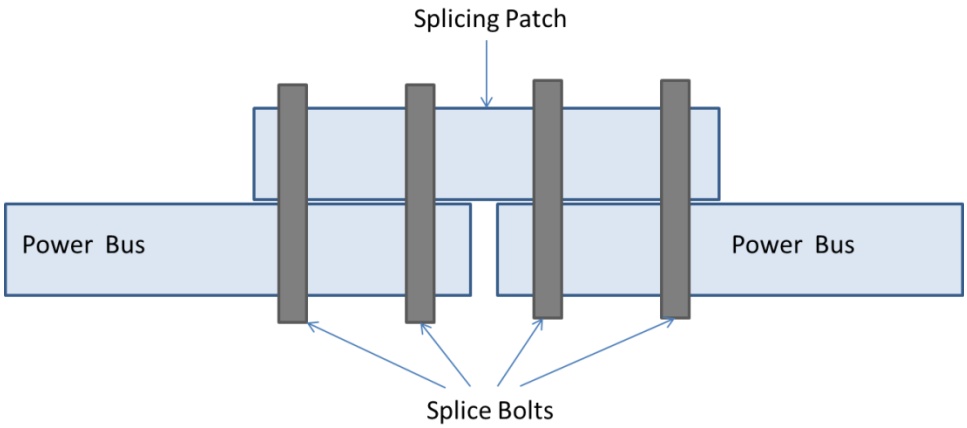

Figure 3-10. Description of Power Bus Splice.

The splice interface is not optimized for contact quality. In other words, the ratio of actual contact area to apparent contact area is very small. Since the amount of actual contact area is so small, fretting wear, and potential subsequent oxidation of mating surfaces, is of primary concern in the studied application. Considering the small area of actual contact and the extreme increase in resistance for oxidized copper, this is likely a primary cause of localized heat generation problems that may arise suddenly. Unfortunately, the supplier of industrial automation power distribution networks can only provide guidelines as to how frequently the system is taken offline and does not have direct control over the likelihood of fretting wear occurring in the field. An ideal approach to reducing the development of localized heat generation problems in the field is to optimize the mating contact surfaces of the bus. This could be provided through tighter geometric tolerances on the final bus material.

As described earlier in Section 1.2.3, the bus is cold drawn and then sheared to length. This is an economical process. The flatness of the bus mating surfaces could be enhanced with additional cold work in a press, or with machining. Both suggested options for improving the mating surface are economically unattractive due to the external costs of adding additional processing to an entire family of parts, of which each part is made in many thousands, annually. The bus bar is a basic component in a very large number of assemblies. As such there would be a large internal engineering cost, due to the creation and processing of drawing and bill of materials changes and engineering change notices, associated with implementing a change to its processing. To optimize the mating surfaces via additional processing would not be feasible to pursue unless it could

be proven that it would drastically increase the reliability of the splice regarding the onset of problematic localized heating in the field. Based on the literature review portion of this text the author would argue that said increased reliability could be proven experimentally. A short term solution would be for the supplier to work with the customer to custom engineer the distribution network to reduce the number of splices between main power conducting buses on a project-to-project basis.

Chapter 4. Conclusion

4.1 Summary

In summary, there were two main purposes for the implementation of this project. The first was to design and validate a bolt pretension measurement method for *in-situ* measurements in industrial automation power distribution networks. The second was to generate a body of knowledge on the contact resistance behavior of the interface between bolted spliced electrical power distribution buses for a set of product. The author has put particular effort on maintaining the concept that the parameters governing the mechanical behavior of the bolted joint and those governing the electrical properties of the bolted electrical splice are highly process specific. Therefore, they are product specific, as geometrical and process tolerances are governed by the organization using the materials. This project is but a small piece in a much larger body of work that the author is developing.

4.2 Conclusions

A methodology is herein presented which can be used to design, tune, and validate a load cell for making *in-situ* measurements of pretension in bolts. The experimental load cell was validated to make measurements within 10% accuracy of the measurements made by an industry clamping load cell. A modeling equation which predicts pretension as a function of applied torque to the same level of accuracy is presented and compared to a typical calculation used in industry which, for the particular case of interest over-predicts pretension by 150%. For brand new samples of bus material clamped with two bolts it was found that the contact resistance can vary by 170% between negligible pretension and 640 pounds of pretension load. Based on this result it is suggested that a

probable root cause for problematic localized heating of the bus is an increase in contact resistance across the splice due to stress relaxation of the bolt. Data on the stress relaxation of medium carbon steels is required for further analysis. The mating surfaces of samples of previously in-use bus material were examined and it is determined macro-scale surface abnormality is leading parameter influencing the contact resistance for cold-drawn, sheared, and punched tin-plated copper bus bar. Based on the literature review and understanding that oxidation of the copper surface will increase the local resistance by a factor of 10^{10}, it is suggested that a an additional probable root cause for problematic localized heating in systems which have been brought offline and put back online many times is degraded mating surface quality on the bus bar via fretting corrosion and oxidation.

References

[1] Franklin, G. F., Powell, J. D., and Emami-Naeni, A. (2006). "Feedback Control of Dynamic Systems, 5th Edition." Pearson-Prentice Hall. New Jersey.

[2] Bickford, J. H. (1983). "That Initial Preload – What Happens to It?" Mechanical Engineering, October, 1983.

[3] Shigley, J. E., Mischke, C. R., and Budynas, R. G. (2003). "Mechanical Engineering Design, 7th Edition." McGraw-Hill. New York.

[4] Norman, C. A. (1925). "Principles of Machine Design." Macmillan Company. New York.

[5] Fisher. J. W., and Struik, J. H. (1974). "Guide to Design Criteria for Bolted and Riveted Joints." John Wiley & Sons. New York.

[6] Kolstee, H. (1984). "Machine Design for Mechanical Technology." Holt, Rinehart & Winston. New York.

[7] Chesson, E. Jr. and Munse, W. H. (1965). "Studies of the Behavior of High Strength Bolts and Bolted Joints." Engineering Experiment Bulletin 469. University of Illinois-Urbana.

[8] Fastenal Engineering & Design Services. (2009). "Bolted Joint Design Rev. 3-4-2009." Available at: http://www.fastenal.com/content/feds/pdf/Article%20-%20Bolted%20Joint%20Design.pdf. Accessed 2/1/2013.

[9] Philpot, T. (2013). "Mechanics of Materials: An Integrated Learning System, Third Edition." John Wiley & Sons. New Jersey.

[10] Croccolo, D., De Agostinis, M., Vincenzi, N. (2012). "Influence of Tightening Procedures and Lubrication Conditions on Titanium Screw Joints for Lightweight Applications." Tribology International. 55. Pp. 68-76.

[11] Croccolo, D., De Agostinis, M., and Vincenzi, N. (2010). "Failure Analysis of Bolted Joints: Effect of Friction Coefficients in Torque-Preloading Relationship." Engineering Failure Analysis. 18. Pp. 364-373.

[12] Eccles, W., Sherrington, I., and Arnell, R. D. (2010). "Frictional Changes During Repeated Tightening of Zinc Plated Threaded Fasteners." Tribology International. 43. Pp. 700-707.

[13] Stevenson, M. E., McDougall J. L., and Cline, K. G. (2003). "Metallurgical Failure Analysis of Titanium Wing Attachment Bolts." Practical Failure Analysis. 3(4).

[14] Holm, R. (1981). "Electrical Contacts, Theory and Application, 4th Edition." Springer-Verlag. New York.

[15] Braunovic, M., Konchits, V., and Myshkin, N. (2007). “Electrical Contacts: Fundamentals, Applications, and Technology.” CRC Press. Boca Raton, FL.

[16] Timsit, R. (1999). “Electrical Contact Resistance: Fundamental Principles.” in Electrical Contacts, Ed. Paul Slade. Marcel Dekker. New York

[17] Li, L., Song, W., Zhang, G., and Jia, D. (2012). “An Electrical Contact Resistance Model Including Roughness Effect for a Rough MEMS Switch.” J. Micromech. Microeng. 22.

[18]Guo, Z. J., McGuer, N. E. and Adams, G. G. (2007). “Modeling, Simulation and Measurement of the Dynamic Performance of an Ohmic Contact, Electrostatically Actuated RF MEMS Switch.” J. Micromech. Microeng. 17.

[19] Arrazat, B., Duvivier, P. Y., Mandrillon, V. and Inal, K. (2011). “Discrete Analysis of Gold Surface Asperities Deformation Under Spherical Nano-Indentation Towards Electrical Contact Resistance Calculation.” Proceeds of the 57th IEEE Holm Conference on Electrical Contacts. Pp298-302.

[20] Vogler, M. and Sheppard, S. (1993). “Electrical Contact Resistance under High Loads and Elevated Temperatures.” Welding Research Supplement to the Welding Journal. 1993. Pp. 231-238.

[21] Greenwood, J. A. and Williamson, J. B. P. (1966). “The Contact of Nominally Flat Surfaces.” Proceeds of the Royal Society of London A. 295. Pp. 300-319.

[22] Nayak, P. R. (1971).”Random Process Model of Rough Surfaces.” ASME Journal of Lubrication Technology. 93. Pp. 398-407.

[23] Jang, Y. H. and Barber, J. R. (2003) ”Effect of Contact Statistics on Electrical Contact Resistance.” Journal of Applied Physics. 11, 94.

[24] Ciavarella, M., Demelio, G., Barber, J. R. and Jang, Y. H. (2000). ”Linear Elastic Contact of the Weierstrass Profile.” Proceeds of the Royal Society of London A. 456. Pp. 387-405.

[25] Barber, J. R. (2002). “Bounds on the Electrical Resistance between Contacting Elastic Rough Bodies.” The Royal Society of London A. 459. 53-66.

[26] American Society for Testing and Materials. (2011). “Standard Specification for Copper, Bus Bar, Rod, and Shapes and General Purpose Rod, Bar, and Shapes.” ASTM International. West Conshohocken, PA.

[27] Antler, M. (1999). “Materials, Coatings, and Platings” in Electrical Contacts, Ed. Paul Slade, Marcel Dekker. New York.

[28] Safranek, W. H. (1974). “The Properties of Electrodeposited Metals and Alloys: A Handbook.” Elsevier. New York

[29] Zeren, A., and Zeren, M. (2003). "Stress Relaxation Properties of Prestressed Steel Wires." Journal of Materials Processing Technology, 141, 1.pp. 86-92.

[30] Braunovic, M., Konchits, V., and Myshkin, N. (2007). “Electrical Contacts: Fundamentals, Applications, and Technology.” CRC Press. Boca Raton, FL.

[31] Mott, Robert. (2004). “Machine Elements in Mechanical Design, 4th Edition.” Pearson-PrenticeHall. Upper Saddle River, NJ

[32] Bryant, M. (1994). “Resistance Buildup in Electrical Connectors Due to Fretting Corrosion of Rough Surfaces.” IEEE Transactions on Components, Packaging, and Manufacturing Technology-Part A. 17. 1. Pp. 86-95.

[33] Antler, M. (1985). “Survey of Contact Fretting in Electrical Connectors.” IEEE Transactions on Components, Hybrids, and Manufacturing Technology. 8. 1. Pp. 87-104.

[34] American Society of Mechanical Engineers. (2012). “Round Head Bolts (Inch Series). B18.5 – 2012.” American Society of Mechanical Engineers.

[35] American Society of Mechanical Engineers. (2003). “Unified Inch Screw Threads, (UN and UNR Thread Form. B1.1 – 2003.” American Society of Mechanical Engineers.

[36] Poupitch, Ougljesa. “Lock Washer and Fastener Assembly.” U.S. Patent 3,221,792. Filed April 8, 1963. Issued December 7, 1965.

[37] Vishay Micro-Measurements. (2005). Instruction Bulletin B-127-14. Strain Gage Installations with M-bond 200 Adhesive.” Available at: http://www.me.ua.edu/me360/PDF/Strain_Gage_Installations_with_M-Bond_200_Adhesive.pdf Accessed: 2/1/2013.

[38] Hoffman, K. “Applying the Wheatstone Bridge Circuit. W1569-1.0 en.” HBM. Available at: http://www.hbm.com.pl/pdf/w1569.pdf. First accessed 2/1/2013.

[39] DATAQ Instruments, Inc. (2012). “DI-710 Series 16-Channel USB or Ethernet Data Logger, User’s Manual, Manual Revision X.” Akron, Ohio. Available at: https://www.google.com/url?sa=t&rct=j&q=&esrc=s&source=web&cd=1&cad=rja&ved=0CEYQFjAA&url=http%3A%2F%2Fwww.dataq.com%2Fsupport%2Fdocumentation%2Fpdf%2Fmanual_pdfs%2Fdi710_manual.pdf&ei=AJt2UcnVEMjQ2AWaj4C4Cg&usg=AFQjCNHkRqd2P5v0-cLMKG4rvG4DHWHU3g&sig2=r63Am5nVBplqcZY-ZNyZcw&bvm=bv.45512109,d.b2I. First accessed: 2/15/13.

[40] Mott, Robert. (2004). “Machine Elements in Mechanical Design, 4th Edition.” Pearson-PrenticeHall. Upper Saddle River, NJ.

[41] Ciavarella, M., Murolo, G., Demelio, G., and Barber, J. R. (2003). “Elastic Contact Stiffness and Contact Resistance for the Weirstrass Profile.” Journal of the Mechanics and Physics of Solids. 52. Pp. 1247-1265.

[42] Matula, R. A. (1979). “Electrical Resistivity of Copper, Gold, Palladium, and Silver.” Journal of Physical Chemistry, Reference Data. (8,4). Pp. 1147-1298.

[43] Incropera, F., Dewitt, D., Bergman, T., and Lavine, A. (2007). “Fundamentals of Heat and Mass Transfer, Sixth Edition.” John Wiley & Sons, Inc. New Jersey.

[44] Vliet, G. C. and Liu, C. K. (1969). “An Experimental Study of Turbulent Natural Convection Boundary Layers.” J. Heat Transfer. 91. Pp. 517-531.

[45] Bejan, A. (2004). "Convection Heat Transfer, Third Edition." John Wiley & Sons, Inc. New Jersey.

Appendix A: Geometry of Custom Tensile Grips

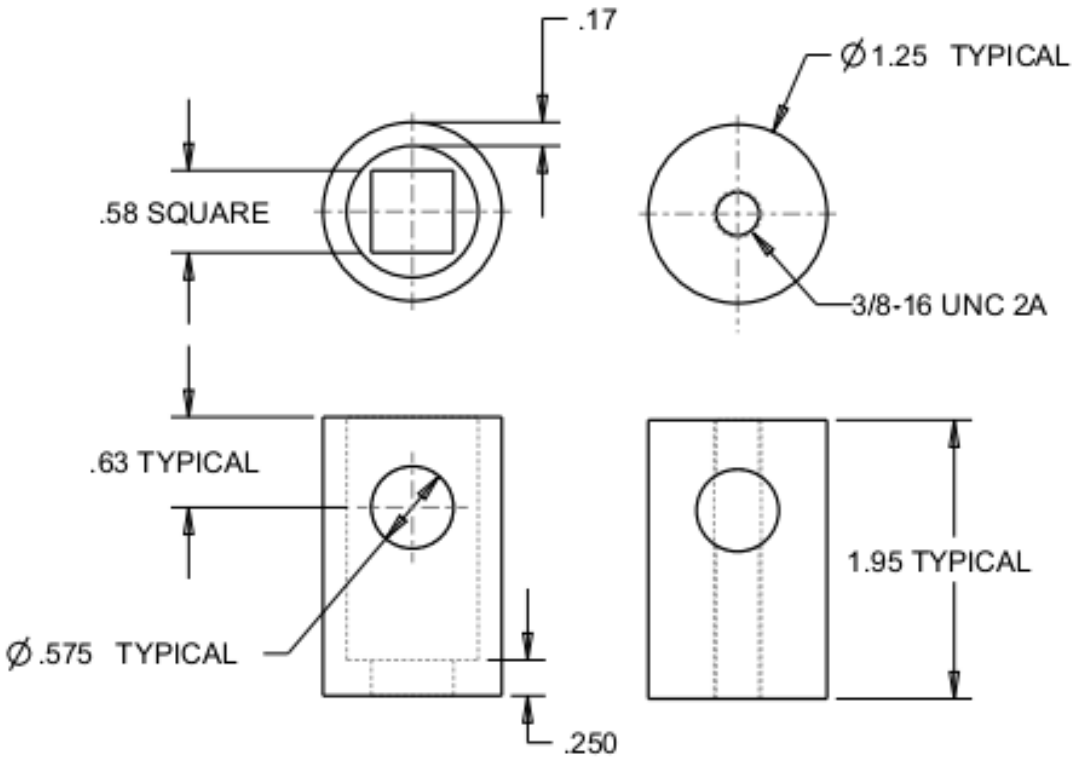

Appendix B: MATLAB Script for Tensile Test Processing

```
%Automated Data Processor for Tensile Test Data on Bolts.


windowOfInterest = 375;
AverageData = zeros(windowOfInterest,3);
numberOfSamples = 9;
AverageYield = 140; %ksi

for i=1:10



    S = num2str(i);
    fileName = strcat('BoltFail',S,'.csv');
    fid=fopen(fileName);
    data = textscan(fid,'%f %f %f
%f','HeaderLines',3,'Delimiter',',','CollectOutput',1);
    fclose(fid)

    data = data{1};

    data = [data(:,3) data(:,2) data(:,4)
zeros(length(data),1)];
    %[ (Strain) (Stress) (Load) (Stress-Strain Slope)]



    %Compute the slope of the stress strain plot.
    for j=2:length(data)
        data(j-1,4) = (data(j,2)-data(j-1,2))/(data(j,1)-
data(j-1,1));
    end

    data(windowOfInterest+1:length(data),:) = [];


    AverageData(:,1) = AverageData(:,1) + data(:,1);
    AverageData(:,2) = AverageData(:,2) + data(:,2);
    AverageData(:,3) = AverageData(:,3) + data(:,4);

    switch i
        case 1
            lineColor = [1 1 0]; %yellow;
        case 2
```

```
            lineColor = [1 0 1]; %magenta;
        case 3
            lineColor = [0 1 1]; %cyan;
        case 4
            lineColor = [1 0 0]; %red;
        case 5
            lineColor = [0 1 0]; %green;
        case 6
            lineColor = [0 0 1]; %blue;
        case 7
            lineColor = [0 0 0]; %black;
        case 8
            lineColor = [.7014 0 1]; %violet;
        case 9
            lineColor = [1 0.2706 0]; %red-orange;
        otherwise
            lineColor = [1 0.4964 0.1367]; %brown;

    end

    data(:,2) = data(:,2)/1000; %convert to Ksi
    data(:,4) = data(:,4)/1000; %convert to Ksi

    figure(222)
    title ('Load vs. Strain Curves, Machined Specimens')
    ylabel('Load (Lbf)')
    xlabel('Strain')
    hold on
    plot(data(:,1),data(:,3),'Color',lineColor)
    hold off

    %convert load data array to percentage of yield stress
    data(:,3) = data(:,2)/AverageYield;

    figure(333)
    title ('Stress vs. Strain Curves, Machined Samples')
    ylabel('Stress (ksi)')
    xlabel('Strain')
    hold on
    plot(data(:,1),data(:,2),'Color',lineColor)
    hold off

    %configure to plot 'modulus' data against % of yield
stress
    modCounter = 0;
    for j = 1:length(data)
        if data(j,3)<1.0
```

```
            modCounter = modCounter+1;
        else
            break
        end
    end


    figure(444)
    title ('Slope of Stress-Strain Curve, Machined
Samples')
    ylabel('"Modulus" (ksi)')
    xlabel('% of Average Yield Stress')
    hold on

plot(data(1:modCounter,3)*100,data(1:modCounter,4),'Color',
lineColor)
    hold off

    %figure(i)
    %plot(data(:,1),data(:,2),data(:,1),data(:,3))



end

AverageData = AverageData/numberOfSamples;

outputFileName = 'AveragedDataMach.csv';
outputFile = fopen(outputFileName, 'w');
fprintf(outputFile,'Strain , Stress , Modulus\n');

for i=1:length(AverageData)
    fprintf(outputFile,'%12.8f , %12.8f , %12.8f\n',
AverageData(i,1),AverageData(i,2),AverageData(i,3));
end

                    fclose(outputFile);
```

Appendix C: MATLAB Script for Compression Test Processing

```
%Automated Data Processor for Compression Test on Nuts.

windowOfInterest = 350;
AverageData = zeros(windowOfInterest,3);
numberOfSamples = 7;

for i=1:numberOfSamples

    S = num2str(i);
    fileName = strcat('Sample',S,'.csv');
    fid=fopen(fileName);
    data = textscan(fid,'%f
%f','HeaderLines',3,'Delimiter',',','CollectOutput',1);
    fclose(fid);

    data = data{1};

    data = [data zeros(length(data),1)];
    %[ (Deformation) (Load) (Load-Deformation Slope)]

    lengthOfData=length(data)

    for j=2:length(data)
        data(j,3) = (data(j,2)-data(j-1,2))/(data(j,1)-
data(j-1,1));
    end

    if i<windowOfInterest+1
        AverageData(:,1) = AverageData(:,1) +
data(1:windowOfInterest,1);
        AverageData(:,2) = AverageData(:,2) +
data(1:windowOfInterest,2);
        AverageData(:,3) = AverageData(:,3) +
data(1:windowOfInterest,3);
    end

    switch i
        case 1
            lineColor = [1 1 0]; %yellow;
        case 2
            lineColor = [1 0 1]; %magenta;
        case 3
            lineColor = [0 1 1]; %cyan;
        case 4
```

```
            lineColor = [1 0 0]; %red;
        case 5
            lineColor = [0 1 0]; %green;
        case 6
            lineColor = [0 0 1]; %blue;
        case 7
            lineColor = [0 0 0]; %black;
        case 8
            lineColor = [.7014 0 1]; %violet;
        case 9
            lineColor = [1 0.2706 0]; %red-orange;
        otherwise
            lineColor = [1 0.4964 0.1367]; %brown;

    end

    data(:,2) = data(:,2)/1000;
    data(:,3) = data(:,3)/1000;

    figure(222)
    title ('Load Profiles')
    ylabel('Load (kip)')
    xlabel('Deformation (in)')
    hold on
    plot(data(:,1),data(:,2),'Color',lineColor)
    hold off

    figure(444)
    title ('Slope of Load Profiles')
    ylabel('"Modulus" (kip/in)')
    xlabel('Load (kip)')
    hold on
    plot(data(:,2),data(:,3),'Color',lineColor)
    hold off

    %figure(i)
    %plot(data(:,1),data(:,2),data(:,1),data(:,3))



end

AverageData = AverageData/numberOfSamples;
AverageData(:,2) = AverageData(:,2)/1000;
AverageData(:,3) = AverageData(:,3)/1000;

figure(222)
```

```
hold on
plot(AverageData(:,1),AverageData(:,2),'--k','LineWidth',3)
hold off

figure(444)
hold on
plot(AverageData(:,2),AverageData(:,3),'--k','LineWidth',3)
hold off

outputFileName = 'AveragedData.csv';
outputFile = fopen(outputFileName, 'w');
fprintf(outputFile,'Deformation , Stress , Modulus\n');

for i=1:length(AverageData)
    fprintf(outputFile,'%12.8f , %12.8f , %12.8f\n',
AverageData(i,1),AverageData(i,2),AverageData(i,3));
end

fclose(outputFile);
```